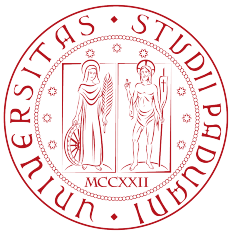

Università degli studi di Padova

Dipartimento di Ingegneria dell'Informazione

Corso di laurea magistrale in Bioingegneria

Quantitative imaging of the GABA-A receptor complex with positron emission tomography data

Relatore: Dott.ssa Alessandra Bertoldo

Correlatori: Dott.ssa Gaia Rizzo
Ing. Matteo Tonietto

Laureando: Emanuele Bello

9 Dicembre 2014

Contents

1 Introduction **3**

2 Material and methods **5**
2.1 PET data 5
2.2 Models 7
2.2.1 Linear spectral analysis 7
2.2.2 Non-linear spectral analysis 8
2.2.3 Two-tissue compartment model 9
2.2.4 Simplified reference tissue model 10
2.2.5 Quantification of the parameters of interest 10
2.3 Estimators 12
2.3.1 ROI level 12
2.3.2 Voxel level 15
2.4 Genomic integration 15
2.5 Statistical analysis 16

3 Quantification results: spectral methods **18**
3.1 Model order 18
3.2 Fit and weighted residuals 19
3.3 Spectrum 24
3.4 Volume of distribution 26
3.5 Placebo-zolpidem data set 32
3.6 Discussion and conclusion 36

4 Quantification results: model-driven methods **37**
4.1 Comparison 3-TCM and 2-TCM 37
4.2 Quantification results of 2-TCM 40
4.2.1 Fit and weighted residual 40
4.2.2 Volumes of distribution 41
4.2.3 Placebo-zolpidem data set 44
4.3 Genomic integration 47
4.3.1 mRNA data 49
4.3.2 Correlations between GABRA and volumes of distribution 50
4.4 Discussion and conclusion 54

5 Quantification results: simplified reference tissue model **55**
5.1 Discussion and conclusion 60

6 Voxel-wise results **62**

7 Conclusion **64**

A Region list **65**
A.1 PET atlas region list 65
A.2 Region of interest list 67
A.3 Allen atlas coarse regions 67
A.4 PET region of interest and Allen region relation 68

B Genomic integration histograms **69**
B.1 Total volume of distribution 69
B.2 First partial volume of distribution 71
B.3 Second partial volume of distribution 73

Bibliography **75**

Chapter 1

Introduction

Receptors for the major inhibitory neurotransmitter, γ-aminobutyric acid (GABA), are divided in two main classes: GABA-A and GABA-B receptors [1]. The majority of GABA-A receptors are composed of α, β and γ subunits: α-subunit class has six members numbered from one to six [2]. These receptors are important drug targets representing the sites of action of benzodiazepines, barbiturates, and neurosteroids [3] and for this reason they have been widely studied [1–7].

Receptor complexes in the brain can be quantified with positron emission tomography (PET), which is a method that allows to measure their in vivo distribution with high resolution and sensitivity [8].

With the additional use of tracer kinetic modeling techniques, it is possible to improve the kind and the quality of information that can be extracted from these biological data [9]: various physiological parameters of interest can be obtained as, for example, volume of distribution (V_t), plasma to tissue rate constant (K_1), irreversible rate constant (K_i) and binding potential (BP).

Two PET ligands, [^{11}C]flumazenil and [^{11}C]Ro15-4513, are mainly used for in vivo neurochemical imaging of the human GABA system and both bind to the benzodiazepine site on the GABA-A receptor [10].

In this thesis [^{11}C]Ro15-4513 will be studied: it has a relative selectivity for the α_5 subtype of the GABA-benzodiazepine receptor [11]. However, the concentration of the tracer does not accurately describe the distribution of α_5 subtype because α_1, α_2 and α_3 subtypes are more expressed in the brain and their affinities for the tracer are not negligible. Therefore, mathematical methods are then necessary to isolate the kinetics and the parameters of interest related to receptors containing α_5 subunit.

The aim of this study is to find a quantification method that allows to separate the contributions of different subtypes.

Spectral analysis has been proposed by Myers and colleagues as one of the most promising methods. According to [12], a fast kinetic component,

attributed to α_1 subtype, and a slow one, attributed to α_5 subtype, can be identified and thus partial volumes of distribution can be calculated.

The purpose of the first part of this study is to evaluate and compare the results obtained with model driven and data driven methods including spectral analysis.

Afterwards, a data set containing subjects who were administered zolpidem will be studied: zolpidem is a non-benzodiazepine hypnotic drug that enhances GABA effects and it has a relative selectivity for α_1 subtype. It acts as a blocker for α_1 subtype and thus its contribution to the biodistribution and the kinetics of [^{11}C]Ro15-4513 should decrease.

As regards this second data set, model driven and data driven methods will also be applied to test their ability to extract information about α_5 receptors.

Chapter 2

Material and methods

2.1 PET data

Two different data sets (made available by Imperial college, Department of Neuroscience, London) previously studied in [10] and [12] are considered.

Healthy data set Four healthy male participants (41.5 ± 4.4 years) complete two [^{11}C]Ro15-4513 PET scans with interval of 16.2 ± 5.1 days.

All participants provide written informed consent to take part in the study which is approved both by the Hammersmith Research Ethics Committee and the Administration of Radioactive Substances Advisory Committee, UK.

For further information about healthy data set Stokes and colleagues may be consulted [10].

Placebo-Zolpidem data set Five healthy male volunteers (age mean ± sd: 44 ± 6 years) undergo 2 PET scans at least a week apart, after zolpidem or placebo, the order of which is randomised (double blind protocol).

Zolpidem (20 mg) or an identical placebo is administered 90 minutes before radioligand injection and at the start of the PET scan. Plasma zolpidem levels are measured at the time of PET ligand injection.

For further information about placebo-zolpidem data set Myers and colleagues may be consulted [12].

For all subjects of both datasets, [^{11}C]Ro15-4513 PET images, arterial samples and magnetic resonance images are taken.

[^{11}C]Ro15-4513 PET imaging A bolus injection of [^{11}C]Ro15-4513 (mean ± s.d.: healthy data set 479.6 MBq ± 25.6, placebo-zolpidem data set 495±18 MBq in 3.3 ± 0.49 mL) is administered through an intravenous cannula sited in the dominant antecubital fossa vein. In the placebo-zolpidem data set, no

differences in cold mass injected between scans are found with paired t-tests (mean ± s.d.: 3.22 ± 0.86 μg to 4.30 ± 3.71 μg, t=0.579, P>0.5).

A Siemens ECAT EXACT HR+ (CTI/Siemens, model 962; Knoxville, TN, USA) scanner with an axial field of view of 15.5 cm is used.

A total of 63 transaxial images planes are acquired as 2.42-mm slices with a reconstructed axial resolution of 5.4 mm and a transaxial resolution of 5.6 mm.

[^{11}C]Ro15-4513 scans comprise 24 dynamic time frames (1 x 30, 4 x 15, 4 x 60, 2 x 150, 10 x 300, 3 x 600 seconds) of data which are all corrected for attenuation, random coincidences, scatter error and radioactive decay.

Arterial sampling Each subject has a radial arterial cannula inserted in the non-dominant wrist to allow continuous counting of blood radioactivity concentration for the first 15 minutes of the experiment.

Discrete samples are also taken 4, 6, 8, 10, 20, 35, 50, 65, 80 and 90 minutes after injection. An aliquot of each discrete sample is rapidly centrifuged to obtain corresponding plasma and radioactivity concentrations.

Magnetic resonance imaging All participants undergo a structural T1 MRI scan for coregistration purposes.

As regards healthy data set, MRI scans are acquired using a 3 T Intera Philips Medical System (TR = 9.6 ms, TE = 4.6 ms, flip angle = 8 grades, NSA = 1, voxel dimensions 0.94 x 0.94 x 1.2 mm^3).

In the placebo-zolpidem data set, all subjects have T1-weighted magnetic resonance imaging with a Philips 1.5-T Gyroscan Intera scanner (Philips, Best, The Netherlands).

Preprocessing For each subject, the segmentation of T1 magnetic resonance images is obtained using a multiatlas approach, as described in [13], from 20 Hammers atlases (Copyright Imperial College of Science, Technology and Medicine 2007. All rights reserved) in order to define 67 regions (Appendix A.1). Afterwards, 18 regions of interest are obtained as combination of the 67 regions defined, for more information Appendix A.2 may be consulted. Finally, these ROIs are placed on the [11C]Ro15-4513 images using an affine transformation between the MRI image and the average PET image.

The arterial input function $C_p(t)$ ($[kBq/mL]$) is calculated from the blood concentration and subsequently metabolite corrected, thus:

$$C_p(t) = C_b(t) \cdot POB(t) \cdot PPf(t) \tag{2.1}$$

where $C_b(t)$ ($[kBq/mL]$) is the blood concentration of the tracer, $POB(t)$ ($[unitless]$) is the plasma over blood fraction and $PPf(t)$ ($[unitless]$) is the plasma parent fraction. $POB(t)$ and $PPf(t)$ are fitted applying the function proposed in [14], and the parameters of $PPf(t)$ are calculated using a non-linear mixed effect approach [15]. Afterwards, $C_p(t)$ is fitted with a $Feng^{\otimes}rect$ model [16] (where $\otimes$ indicates the convolution operator) and decay corrected.

2.2 Models

2.2.1 Linear spectral analysis

Spectral analysis (SA, Cunningham and colleagues [17]) is a data driven method that describes the system impulse response function (IRF) as a positive sum of decaying exponentials. This technique allows the description of the tissue time-activity curve of a tracer in terms of an optimal subset of kinetic components selected from a far larger set [18]. Only few assumptions have to be fulfilled in order to apply this method [19].

IRF can be written as:

$$IRF(t) = \sum_{i=1}^{N} \alpha_i \cdot e^{-\beta_i t} \quad with \quad \alpha_i, \beta_i \geq 0, \ \forall i \tag{2.2}$$

where N is unknown while α_i $[mL/cm^3\, min]$ and β_i $[min^{-1}]$ have to be estimated.

The concentration in the tissue ($C_t(t)$ $[kBq/cm^3]$) is obtained as a convolution between the $C_p(t)$ and the $IRF(t)$. In addition, $C_b(t)$ is used to describe the blood part of the signal.

Therefore, the concentration of the tissue can be written as:

$$\begin{aligned} C_t(t) &= (1 - V_b) \cdot C_p(t) \otimes IRF(t) + V_b \cdot C_b(t) \\ &= (1 - V_b) \cdot \sum_{i=1}^{N} \alpha_i \cdot \int_0^t C_p(\tau) e^{-\beta_i \cdot (t-\tau)} d\tau + V_b \cdot C_b(t) \\ &with \quad \alpha_i, \beta_i \geq 0, \ \forall i \end{aligned} \tag{2.3}$$

where V_b $[unitless]$ is the volume of blood in the region or voxel.

The estimation problem is non-linear in the parameters β_i and the number of exponential terms is unknown. However, if we define a grid containing a large number, M, of β_i values it is possible to postulate the estimation problem as:

$$C_t(t) = (1 - V_b) \sum_{i=1}^{M} \alpha_i \cdot C_i(t) + V_b \cdot C_b(t) \tag{2.4}$$

where $C_i(t)$ is the convolution of $C_p(t)$ with the exponential term $e^{-\beta_i t}$.

The new estimation problem is linear in the parameters but it is overcomplete because M (≥ 100) is much greater than N. Therefore, the estimation of the coefficients α_i from Equation 2.4 requires non-negativity constraints on α_i to avoid inclusion of pairs of nearly equal components with coefficients opposite in sign [18]. Weighted linear non-negative least square can be used to estimate α_i values.

α_i and β_i values can be plotted, respectively, on y and x axis to obtain the "spectrum": the number of lines is equal to the number of exponential terms and thus to the number of compartments. High frequency lines, that is the higher βs, are related with blood kinetics while low frequency lines, i.e. β_is near zero, identify the slow components of the tracer, where β_i=0 indicates the presence of an irreversible trapping component in the tissue.

SA does not need prior information about the number of compartments therefore it is usually used for preliminary analysis. However, only the number and the types of compartments are obtained: compartmental models are needed to find the correct structure.

V_t $[ml/cm^3]$, K_1 $[mL/cm^3\,min]$ and K_i $[mL/cm^3\,min]$ can be calculated from α_i and β_i values. Volume of distribution is formulated as:

$$V_t = \sum_{i=1}^{M} \frac{\alpha_i}{\beta_i} \tag{2.5}$$

Instead, K_1 and K_i can be formulated as:

$$K_1 = \sum_{i=1}^{M} \alpha_i \tag{2.6}$$

$$K_i = \alpha_0 \tag{2.7}$$

where α_0 is non-zero if an irreversible compartment is found.

2.2.2 Non-linear spectral analysis

Non-linear spectral analysis (NLSA, Bertoldo and colleagues [20]) is a data-driven method that describes the impulse response function in the same way of the LSA that is a positive sum of decay exponentials (Equation 2.2).

However, the number and the types of compartments have to be chosen a priori: it is a limitation but it avoids overfitting and differences in the number of compartments found between regions.

In particular, in NLSA a set of model alternatives is defined a priori (fixing the number of exponentials to a predefined range of values) and then compared.

Macroparamaters can be obtained from α and β values through equations presented in section 2.2.1. If the model contains irreversible compartment, K_i can be calculated and it is equal at the α value of the trapping component. For example, 2-exponential V_t is reported:

$$V_t = \frac{\alpha_1}{\beta_1} + \frac{\alpha_2}{\beta_2} \tag{2.8}$$

2.2.3 Two-tissue compartment model

Two-tissue compartment model (2-TCM, Mintun and colleagues [21]) is a model with two reversible compartments connected in series, see Figure 2.1.

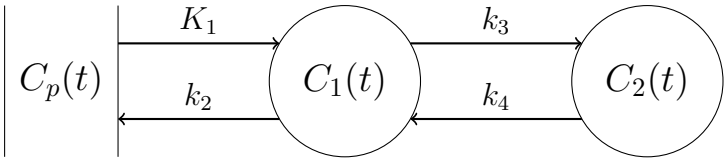

Figure 2.1: Two-tissue compartment model

It is described by a system of differential equations:

$$\frac{dC_1(t)}{dt} = -(k2 + k3) \cdot C_1(t) + k4 \cdot C_2(t) + K_1 \cdot C_p(t) \tag{2.9}$$

$$\frac{dC_2(t)}{dt} = +k3 \cdot C_1(t) - k4 \cdot C_2(t) \tag{2.10}$$

$$C_t(t) = (1 - V_b) \cdot (C_1(t) + C_2(t)) + V_b \cdot C_b(t) \tag{2.11}$$

where V_b is the blood volume and $C_b(t)$ is the concentration of tracer in the blood.

This model is widely used in PET receptor studies and the tracer's concentration can be usually described as follows:

- the first compartment, $C_1(t)$, describes free tracer and non-specifically bound tracer kinetics.
- the second compartment, $C_2(t)$, describes specific bound tracer kinetics.

$C_1(t)$ kinetics is usually faster than $C_2(t)$ kinetics because free and non-specific binding are fast phenomena.

Macroparameters can be estimated from kinetic parameters and V_t is given by:

$$V_t = \frac{K_1}{k_2}\left[1 + \frac{k_3}{k_4}\right] \tag{2.12}$$

In addition to V_t and K_1, another macroparameter, called non displaceable binding potential (BP_{ND}) [*unitless*], can be calculated as:

$$BP_{ND} = \frac{k_3}{k_4} \tag{2.13}$$

In general, a greater amount of BP is explained with a greater amount of receptors.

2.2.4 Simplified reference tissue model

The quantification of the arterial input function (AIF) requires arterial cannulation, time-consuming metabolite measurements and discomfort for the patient.

In reference tissue models, a region devoid of specific receptors is used as model input.

Lammertsma and colleagues [22] have proposed a simplified reference tissue model (SRTM) which estimates three parameter of interest: BP_{ND}, R_1 $[unitless]$ (which accounts for any differences in delivery to the region of interest and the reference tissue) and k_2 $[min^{-1}]$ that is the rate constant for transfer from tissue to plasma.

The equation of tissue concentration is given by:

$$C_t(t) = R_1 C_r(t) + [k_2 - \frac{R_1 k_2}{1 + BP}] C_r(t) \otimes e^{\frac{-k_2 t}{1+BP}} \tag{2.14}$$

where $C_r(t)$ is the concentration of the tracer in the reference tissue.

In this study, the cerebellum is chosen as reference region due to its lack of α_5 receptors. To note that it contains large amounts of α_1 and α_6 subtypes.

2.2.5 Quantification of the parameters of interest

Different parameters of interest will be considered in this study: V_t, partial V_ts and BP_{ND}.

In fact, the purpose of the analysis is to distinguish the $\alpha_1 \backslash \alpha_5$ contributes. Therefore, two different partial V_ts will be considered following previous results [12]: V_1 (related to α_1 subtype) and V_5 (related to α_5 subtype). These will be calculated differently depending on the method considered.

Total volume of distribution For LSA, 2-exponential NLSA and 2-TCM, V_t will be calculated respectively with Equation 2.5, 2.8 and 2.12.

To note that V_ts calculated with 2-TCM and NLSA are almost equal except for numerical approximation in the estimation: in fact comparing the concentration in the tissue obtained with 2-exponential NLSA

$$C_t(t) = (1 - V_b) \cdot \left[\alpha_1 \cdot C_p(t) \otimes e^{-\beta_1 t} + \alpha_2 \cdot C_p(t) \otimes^{-\beta_2 t}\right] + V_b \cdot C_b(t) \tag{2.15}$$

with that obtained with 2-TCM

$$C_t(t) = (1 - V_b) \left(\frac{K_1}{\beta_2 - \beta_1} \left[(k_3 + k_4 - \beta_1) e^{-\beta_1 t} + (\beta_2 - k_3 - k_4) e^{-\beta_2 t}\right] \otimes C_p(t) \right) + V_b C_b(t) \tag{2.16}$$

where

$$\beta_1 = \frac{(k_2 + k_3 + k_4) - \sqrt{(k_2 + k_3 + k_4)^2 - 4k_2k_4}}{2} \tag{2.17}$$

$$\beta_2 = \frac{(k_2 + k_3 + k_4) + \sqrt{(k_2 + k_3 + k_4)^2 - 4k_2k_4}}{2} \tag{2.18}$$

their similarity results clear.

Partial volumes of distribution For each method, V_1 and V_5 will be obtained as follows: in the spectral methods V_1 is related to the fast component of the spectrum while V_5 to the slow one. As regards 2-TCM, V_1 is the volume of distribution of the first compartment while V_5 of the second one.

Thus, they are formulated as:

$$LSA \begin{cases} V_1 = \sum_{i=1}^{N} \frac{\alpha_i}{\beta_i} \quad with \quad \beta_i \geq \beta_{cutoff} \\ V_5 = \sum_{i=1}^{M} \frac{\alpha_i}{\beta_i} \quad with \quad \beta_1 < \beta_i < \beta_{cutoff} \end{cases} \tag{2.19}$$

where β_{cutoff} will be fixed according to spectrum result and $\beta_1 = 0.001$ $[min^{-1}]$.

$$2 - exponential\, NLSA \begin{cases} V_1 = \frac{\alpha_1}{\beta_1} \\ V_5 = \frac{\alpha_2}{\beta_2} \end{cases} \tag{2.20}$$

where β_1 is the beta with the highest value.

$$2 - TCM \begin{cases} V_1 = \frac{K_1}{k_2} \\ V_5 = \frac{K_1 k_3}{k_2 k_4} \end{cases} \tag{2.21}$$

While total V_t of 2-exponential NLSA and 2-TCM can be compared, V_1 and V_5 are related to different compartments in the two different models.

In the NLSA they are related to the first and to the second exponential:

$$C_1(t) = \alpha_1 e^{-\beta_1 t} \tag{2.22}$$

$$C_2(t) = \alpha_2 e^{-\beta_2 t} \tag{2.23}$$

where $\beta_1 > \beta_2$.

On the other hand, V_1 calculated with 2-TCM is related to the first compartment, i.e. free and non-specific binding, while V_5 to the second that is specific binding (full derivation can be found in [23]):

$$C_1(t) = \frac{K_1}{\beta_2 - \beta_1}\left[(k_4 - \beta_1)e^{-\beta_1 t} + (\beta_2 - k_4)e^{-\beta_2 t}\right] \tag{2.24}$$

$$C_2(t) = \frac{K_1 k_3}{\beta_2 - \beta_1}\left[e^{-\beta_1 t} - e^{-\beta_2 t}\right] \tag{2.25}$$

where β_1 and β_2 are defined in Equation 2.17 and 2.18.

Therefore, the V_1 and V_5 obtained with spectral methods can not be interpreted as free, non-specific or specific binding since model-based methods are needed.

Non displaceable binding potential As regards BP_{ND} calculated with SRTM, it will be compared to three different parameters:

1. BP_{ND} of 2-TCM (Equation 2.13, "direct" estimate).
2. BP_{ND} obtained as:
$$BP_{ND} = DVR - 1 \tag{2.26}$$
where DVR is the distribution volume ratio and it is equal at $DVR = \frac{V_t}{V_{t_{ref}}}$ where V_t is the 2-TCM tissue volume of distribution while $V_{t_{ref}}$ is the volume of distribution of the cerebellum calculated by 1-TCM.
3. V_5 of 2-TCM.

2.3 Estimators

2.3.1 ROI level

Linear spectral analysis

LSA is solved with non-negative weighted-least-square algorithm (lsqnonneg in MATLAB): let y be the TACs measured, G a matrix containing C_i and C_b on the columns (Equation 2.4), Σ_v the error covariance matrix and $\mathbf{p}$ the vector of parameters, the optimization problem can be written as:

$$\min_p \|y - G \cdot \mathbf{p}\|^2_{\Sigma_v^{-1}} \quad \text{with } \mathbf{p} \geq 0 \tag{2.27}$$

PET data measurement error is assumed to be additive and uncorrelated, with zero mean and Gaussian distribution. The error covariance matrix is diagonal (as per standard practice in PET) with variance of the i-th element, $Var(TAC(t_i))$, defined according to the formula originally proposed by Mazoyer and colleagues [24]:

$$Var(TAC(t_i)) = \gamma \frac{TAC(t_i)}{\Delta_{t_i}} \tag{2.28}$$

where $TAC(t_i)$ represents the activity of the radioligand in a specific volume of interest in the frame i, and Δ_{t_i} is the duration of frame i. The proportionality constant γ is an unknown scale factor estimated a posteriori as in [25].

y, G and p can be formulated in the following way:

$$y = \begin{bmatrix} TAC(t_1) \\ \vdots \\ TAC(t_N) \end{bmatrix} \tag{2.29}$$

$$G = \begin{bmatrix} C_1(t_1) & \cdots & C_M(t_1) & C_b(t_1) \\ \vdots & \vdots & \vdots & \vdots \\ C_1(t_N) & \cdots & C_M(t_N) & C_b(t_N) \end{bmatrix} \tag{2.30}$$

where $C_i(t)$ is the concentration of the plasma convolved to the i-th exponential term and

$$\mathbf{p} = \begin{bmatrix} \alpha_1 \\ \vdots \\ \alpha_M \\ V_b \end{bmatrix} \tag{2.31}$$

Some observations:

- t_i is the i-th sampling time, with $i = 1, \cdots, N$,
- M is the number of βs in the grid,
- α values in p vector contain an $(1 - V_b)$ factor which must be removed.

As regards the choice of the beta grid, there are three main choices to make: range, distribution and number of components. Various studies have shown that the log-normal distribution is a convenient choice for most of the tracers and 100 or 200 components are generally sufficient. On the other hand, optimum range depends on the tracer; individual studies are made to investigate this particular feature.

In this thesis two different grids will be tested:

1. range β from 0.001 to 1 $[min^{-1}]$, log-distribution, M=100 components,
2. range β from 0.001 to 1 $[min^{-1}]$, log-distribution, M=1000 components.

Non-linear spectral analysis

In the first part of this thesis, several types of NLSA models will be tested to find which one best describes [^{11}C]Ro15-4513 brain data:

- 1 reversible compartment model (1-exponential),
- 1 reversible compartment and 1 irreversible compartment model (1-exponential with trapping component),
- 2 reversible compartments model (2-exponential),
- 2 reversible compartments and 1 irreversible compartment model (2-exponential with trapping component),
- 3 reversible compartments model (3-exponential).

NLSA is solved with non-linear weighted least square method implemented in home-made MATLAB functions. If y is the TAC measured, $C_t(\mathbf{p})$ is the concentration of tissue calculated with the model, Σ_v is the error covariance matrix and $\mathbf{p}$ is the vector of parameters, the optimization function can be written as:

$$\min_{\mathbf{p}} \|y - C_t(\mathbf{p})\|^2_{\Sigma_v^{-1}} \tag{2.32}$$

where the measurement error is defined as for LSA.

For each model tested, various combinations of initial values are tried in order to achieve the optimum one.

Afterwards, the best model among the five tested, defined as the one with the lowest Akaike information criterion (AIC) under the constraint of having the coefficients of variation (CV) of all parameters lower than 200%, will be compared with other methods.

Two-tissue compartment model

Two-tissue compartment model is solved with the non linear weighted least square estimator as NLSA (Equation 2.32). The assumptions of measurement error are equal to those of the previous methods.

The initial values of parameters required by lsqnonlin are derived from the relationship between 2-TCM and NLSA (Equation 2.15 and 2.16).

Simplified reference tissue model

Simplified reference tissue model is solved with non linear weighted least square method as NLSA and 2-TCM (Equation 2.32) and the same assumptions on the measurement error are made.

2.3.2 Voxel level

Voxel level analysis solves the kinetic models for each element of the image producing parametric maps having the same spatial resolution as the original PET image [26]. Due to the low SNR of the voxel kinetics and very high number of voxels to be analyzed, nonlinear estimators cannot be used [26].

In the past 10 years, various techniques have been proposed to apply nonlinear models at voxel analysis. In this thesis, hierarchical basic function method (HBFM) will be used to obtain parametric maps for 2-exponential NLSA and 2-TCM models. For a detailed description of the method, the interested reader is referred to [26].

The assumptions on the measurement error are equal to those of the previous methods but in this case the error variance is defined as the ratio of the activity of the radioligand in the whole brain over the frame length.

2.4 Genomic integration

The distribution and the quantity of GABA receptors in the different areas of the brain are not known precisely. According to various studies, only relative and semi-quantitative informations are available as, for example, regions with low or high amount of an α subtype. In Table 2.1 the main GABA-A receptors and their quantity are reported.

	Subtype(Composition)			
	α_1 ($\alpha_1\beta_2\gamma_2$)	α_2 ($\alpha_2\beta_n\gamma_2$)	α_3 ($\alpha_3\beta_n\gamma_2$)	α_5 ($\alpha_5\beta_{1/3}\gamma_2$)
Quantity	$\sim 60\%$	$\sim 20\%$	$\sim 15\%$	$\sim 5\%$
[^{11}C]Ro15-4513	10.4	5.5	7.8	0.5
Zolpidem	17	291	357	>15000

Table 2.1: A summary of the distribution of the four "benzodiazepine-sensitive" GABA-A receptor subtypes, and a selection of interacting pharmacological agents [3]. Affinities of these compounds are presented as K_i/nM [27]. Table kindly granted by Jim F. Myers.

The Allen Human Brain Atlas (AHBA) is an anatomically comprehensive atlas of the adult human brain transcriptome, recently made freely available by the Allen Institute for Brain Science [28]. This atlas represents a gene expression survey in multiple adult control brains, in 500 samples per hemisphere. AHBA includes the mRNA information of $>$ 20'000 genes, which can be downloaded from *http://human.brain-map.org/* at different levels of resolution ("sample", one mRNA expression level per sample, "structure", mRNA levels are averaged in 156 regions of interest, and "coarse", where mRNA are reported in 26 macro-regions of interest).

AHBA is used as source of transcriptional mRNA maps for an exploratory analysis of [^{11}C]Ro15-4513 quantification methods using mRNA distribution to identify α_1/α_5 binding.

mRNA data of the genes of interest (GABA receptor α_1, α_2, α_3, α_4, α_5, α_6) are downloaded at "coarse" level and mRNA levels are averaged across the donors, in order to obtain a between-subject mean mRNA profile for each receptor subtype.

2.5 Statistical analysis

To assess methods performance, several indexes are taken in consideration. Non-physiological or non-reliable estimates, defined as V_t with CV higher than 50%, are removed.

Repeatability As regards test-retest healthy dataset, three indexes are used to assess the method repeatability: Pearson's correlation coefficient (R^2), intraclass correlation (ICC) and mean relative difference (MRD).

For each method, R^2 and ICC are calculated for V_t, V_1 and V_5 taking into account all the ROIs of all subjects:

$$R^2 = \left(\frac{\sum_{i=1}^{n} \left(V_{t_{i_{test}}} - \overline{V}_{t_{test}}\right)\left(V_{t_{i_{retest}}} - \overline{V}_{t_{retest}}\right)}{\sqrt{\sum_{i=1}^{n} \left(V_{t_{i_{test}}} - \overline{V}_{t_{test}}\right)^2} \sqrt{\sum_{i=1}^{n} \left(V_{t_{i_{retest}}} - \overline{V}_{t_{retest}}\right)^2}} \right)^2 \tag{2.33}$$

where n is the number of reliable ROIs on all subjects, $V_{t_{i_{test}}}$ and $V_{t_{i_{retest}}}$ are the volumes of distribution of the i-th ROI while $\overline{V}_{t_{test}}$ and $\overline{V}_{t_{retest}}$ are the mean of the volumes of distribution in test and retest.

Instead, ICC is given by:

$$ICC = \frac{MS(bs) - MS(ws)}{MS(bs) + MS(ws)} \tag{2.34}$$

where MS is the mean sum of squares of the volumes of distribution, bs means "between subject" and ws means "within subject".

As regards MRD, the relative difference for each ROI of the subjects is calculated as:

$$RD_i = 100 * \left| \frac{V_{t_{test_i}} - V_{t_{retest_i}}}{\frac{V_{t_{test_i}} + V_{t_{retest_i}}}{2}} \right| \tag{2.35}$$

where $V_{t_{test_i}}$ and $V_{t_{retest_i}}$ are the volumes of distribution of the i-th ROI. Afterwards, mean, i.e. MRD, and standard deviation of the RD_i are separately calculated for each subject.

Impact of zolpidem administration For the placebo-zolpidem data set, the average on the five subjects of the percentage differences (PD) of V_t, V_1 and V_5 between placebo and zolpidem administration are obtained for each ROI:

$$PD = MEAN\left(100 * \frac{V_{t_{placebo}} - V_{t_{zolpidem}}}{V_{t_{placebo}}}\right) \tag{2.36}$$

Lastly, Spearman's rho (ρ) are calculated for each α subreceptor to assess the correlation of mRNA distributions and [^{11}C]Ro15-4513 quantification results.

Chapter 3

Quantification results: spectral methods

In this chapter, NLSA and LSA will be compared in several aspects: model order, fit, weighted residuals, spectrum and repeatability. Furthermore, placebo-zolpidem dataset will be used to study the variation of the volumes of distribution after zolpidem administration.

3.1 Model order

NLSA As regards the non-linear spectral analysis, the five models reported in section 2.3.1 are applied to the healthy dataset. Table 3.1 reports the percentage of the ROIs where each model is selected as optimal according to parsimonia criteria (as described in section 2.3.1).

Model	ROI percentage [%]
1-exponential	15
1-exponential with trapping component	20
2-exponential	53
2-exponential with trapping component	13
3-exponential	0

Table 3.1: Optimal model according to non-linear spectral analysis

In agreement with previous studies, the two components model is identified in the majority of the ROIs (73%, Table 3.1). The 2-exponentials with trapping component model is often selected in the Pallidum (37.5%).

In 33% of the ROIs, a model with trapping component is identified; two explanations can be given to understand this contrasting result:

1. The trapping component improves the fit of the model and so it is found even when the irreversible compartment does not belong to tracer kinetics.

2. The duration of the specific binding is comparable with the length of the PET exam therefore it is identified as an irreversible component.

Mono-exponential model is selected as the optimal one in the 15% of the ROIs especially in the Cerebellum. In the 75% of subjects in fact it provides good fits comparable with those obtained with 2-exponentials. According to Myers and colleagues, in the Cerebellum the one-tissue compartment model fitted TACs almost as well as did the two-tissue compartment model [12].

Based on these results and considerations, two-exponentials model is chosen as the best one for all ROIs except for the Cerebellum in which mono-exponential is selected as the optimal model. As regards Pallidum, two-exponentials is selected as best model although the presence of the trapping component will be taken into account.

LSA LSA identifies a greater number of components than NLSA, results are reported in Table 3.2 (no trapping component is included in the grid).

Number of reversible components	ROI percentage [%]
1	2
2	47
3	42
4	10

Table 3.2: Number of reversible components identified by linear spectral analysis

In the 52% of the ROIs three or more components are found. Furthermore, boundary components, i.e. those with betas equal at 0.001 or 1 $[min^{-1}]$, are identified with high frequency, for example 38% of the ROIs contain a lower-bound component.

Considering the number of components, NLSA is preferable to LSA because it avoids their overestimation.

3.2 Fit and weighted residuals

NLSA The two-exponentials model gives good fits of data with uncorrelated weighted residuals (in Figure 3.1 model fit and weighted residuals of the Insula for a representative subject).

Similar results are obtained in others regions; however some differences can be found:

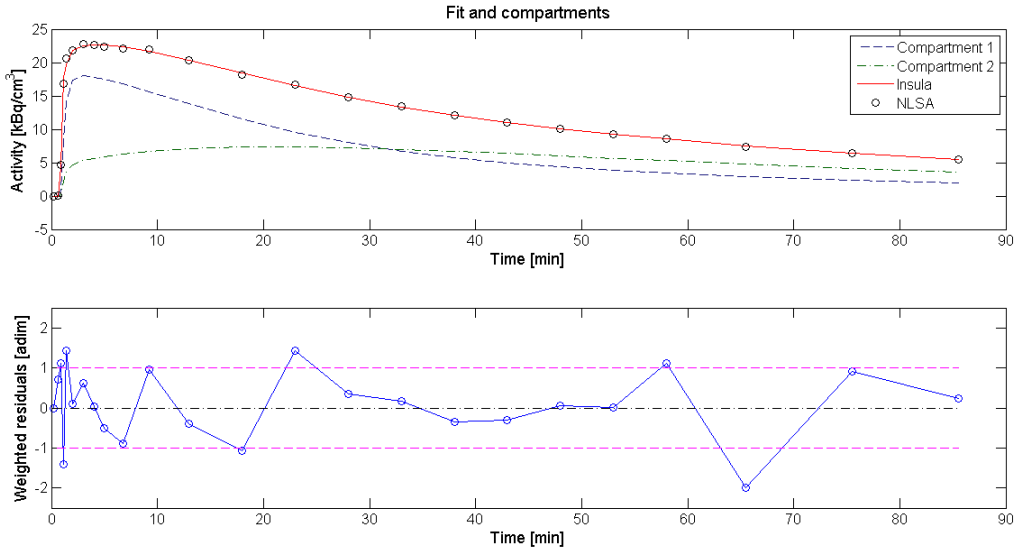

Figure 3.1: Fit, compartments and weighted residuals of Insula by two-exponential NLSA model.

- Accumbens, Amygdala, Cingulate, Hippocampus and Insula have tissue activity curve with slow kinetics.
- Whole brain, Occipital lobe and Thalamus have fast kinetics.
- Pallidum have a high acute peak and a fast wash-out in the majority of the subjects.
- Cerebellum has the fastest kinetics.

These results are in agreement with physiological informations obtained from GABA-A receptor studies: high expression levels are found in limbic area, i.e. Amygdala and Hippocampus, and Accumbens nucleus while lower amounts are reported in Cingulate cortex and Insula. On the other hand, Occipital lobe and Thalamus contain few α_5 receptors and their percentage in whole brain is very low (5%, Table 2.1). Furthermore, the lack of α_5 subunits in the cerebellum explains its fast kinetics and the best fit obtained by one-component model. As regards Pallidum, small amount of α_5 receptors is reported in some studies [6] [7] and thus its fast behaviour is expected, however, the acute peak in the initial part of the curve is unusual. Further information should be taken in consideration, such as anatomical structure, in order to understand its kinetics.

Since the number of compartments is fixed for all regions, some failures of estimation can be obtained with two-exponentials model due to the large variability in the receptors distribution. For example, in the Occipital lobe a one-exponential model might be enough in some subjects and so one component of the two-exponentials model might collapse to a boundary limit such as $\beta = 0.99$ or approximately zero.

In agreement with [12], high inter-subject variability is found due to the complexity of the GABA-A receptor system.

Given the high inter-subject variability, different combinations of the values of the initial parameters are tried for each subject.

The optimal set is:

$$
\begin{aligned}
V_b &= 0.05\,[unitless] \\
\alpha_1 &= 0.3\,[mL/cm^3\,min] \\
\beta_1 &= 0.14\,[min^{-1}] \\
\alpha_2 &= 0.08\,[mL/cm^3\,min] \\
\beta_2 &= 0.04\,[min^{-1}]
\end{aligned}
$$

All estimated blood volumes have physiological value in all subjects and ROI (V_b mean $\pm$ sd: 0.048 $\pm$ 0.012 $[unitless]$).

LSA As regards LSA, fits, compartments and weighted residuals are obtained with the two different grids, the results are reported in Figure 3.2.

The results are grid-dependent:

- with the first grid (range of betas [0.001 1] $[min^{-1}]$ and 100 components) poor fits and weighted residuals are achieved compared to NLSA, see Figure 3.2a. The weighted residuals are correlated and the predicted concentration does not correctly fit the last part of the curve.
- on the other hand, increasing the number of components to 1000 the results become comparable with those of NLSA (see Figure 3.2b and 3.1): weighted residuals become random and uncorrelated and the fit explains the last part of the time activity curve of the tissue.

In LSA, the quantization of the grid significantly affects the goodness-of-fit of [^{11}C]Ro15-4513 human brain data, despite several studies have reported that 100 or 200 components are usually enough to obtain satisfying fits and weighted residuals.

Furthermore, a decrease of CV values is obtained, while there are negligible change in the parameter estimates (results of Insula are reported in Table 3.3).

The biggest difference is related with the slow component (difference of 5% in β_1) and thus the highest improvement in goodness-of-fit is found in the final part of the curve. The same holds in other ROIs.

One of the most significant feature of the LSA is its computational cost: being a linear method it is computationally faster compared to non-linear techniques as NLSA. However, if the number of components is very high this propriety is lost.

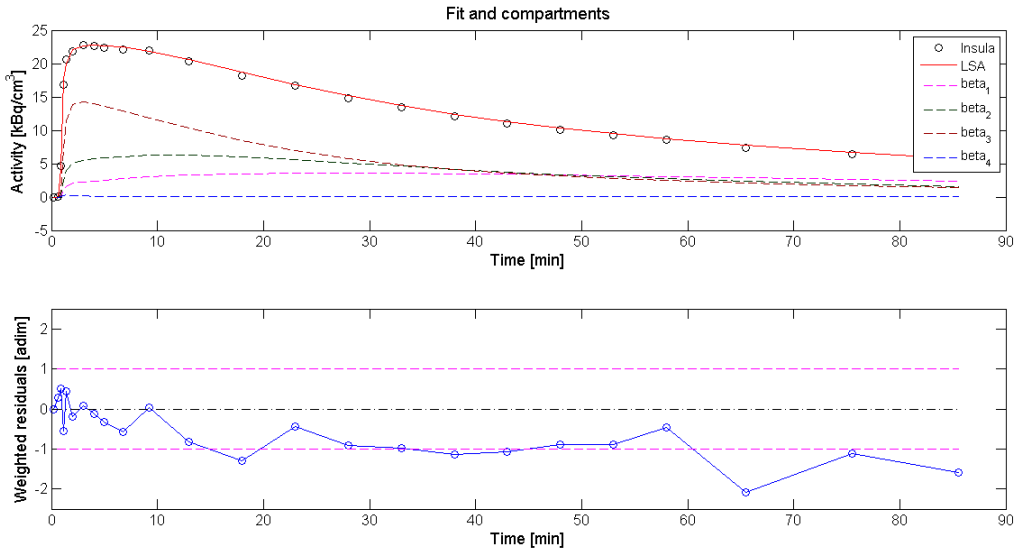

(a) beta grid=[0.001 : 1] $[min^{-1}]$, number of components=100.

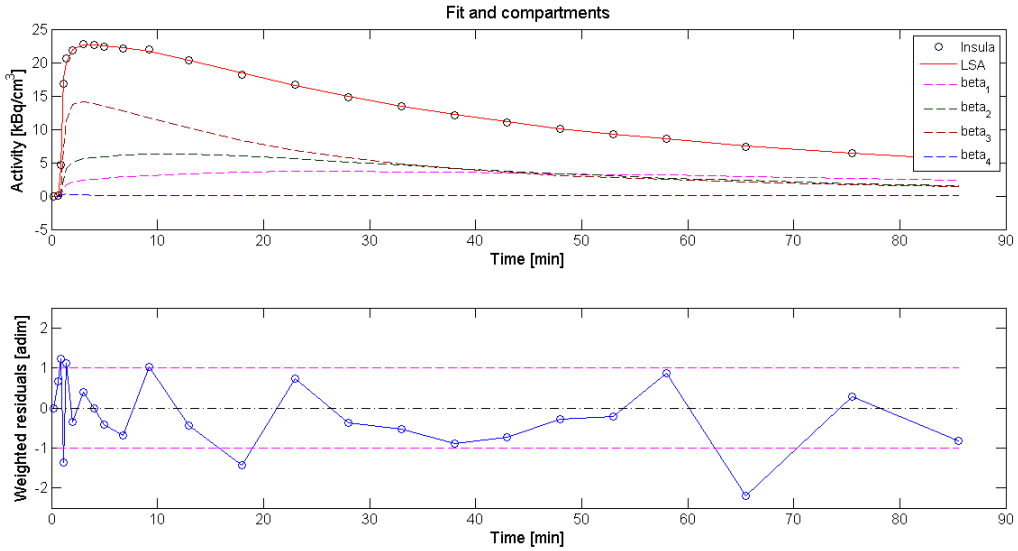

(b) beta grid=[0.001 : 1] $[min^{-1}]$, number of components=1000.

Figure 3.2: Fit, compartments and weighted residuals of Insula by LSA

Parameter	100 components grid	1000 components grid
$\alpha_1\,[mL/cm^3\,min]$	0.029	0.029
CV [%]	10	4
$\beta_1\,[min^{-1}]$	0.019	0.020
$\alpha_2\,[mL/cm^3\,min]$	0.075	0.076
CV [%]	18	7
$\beta_2\,[min^{-1}]$	0.054	0.055
$\alpha_3\,[mL/cm^3\,min]$	0.217	0.215
CV [%]	10	4
$\beta_3\,[min^{-1}]$	0.126	0.127
$\alpha_4\,[mL/cm^3\,min]$	0.006	0.006
CV [%]	466	194
$\beta_4\,[min^{-1}]$	0.726	0.732
$V_b\,[unitless]$	0.050	0.050
CV [%]	19	8
$V_t\,[ml/cm^3]$	4.572	4.574
CV [%]	0.6	0.3
WRSS $[unitless]$	0.0289	0.005

Table 3.3: Difference between parameters and their CV with different grids in Insula

Using 1000 components, the length of LSA analysis is comparable with that of the NLSA and thus non-linear methods are preferable in the ROI level.

Given the little difference between the volumes of distribution calculated and the large increase in computational time, the first grid is chosen as the best one and so it will be used in comparison with NLSA.

As regards the applicability on the different ROIs, LSA is more flexible than NLSA since the number of compartments is not fixed a priori. In fact, LSA adapts the number of components in order to fit the tissue concentration. For example, in the cerebellum the slow component is identified in 13% of the subjects.

On the other hand, as said in the previous section, the number of components found is often higher than necessary. In the Insula this fact is evident: even if LSA identifies four components (Figure 3.2a and Table 3.3) the optimal model according NLSA is the two-exponentials model.

In most ROIs, the CVs of the parameters estimated with LSA are normally comparable with those obtained with NLSA. However, boundary components have very high CVs in both methods.

Considering the fits and the weighted residuals, NLSA is preferable to LSA because it has better goodness-of-fit and its residuals are uncorrelated and random.

3.3 Spectrum

NLSA and LSA spectra can be compared to study their ability to separate the different contributions of α subtypes.

NLSA As regards NLSA, two main components can be identified: a slow one containing the betas in the interval $[0 : 0.09]$ $[min^{-1}]$ and a fast one with the betas greater than 0.09 $[min^{-1}]$ (Figure 3.3). The separation is not clear because the distribution is very compact, in fact most betas are smaller than 0.2 $[min^{-1}]$.

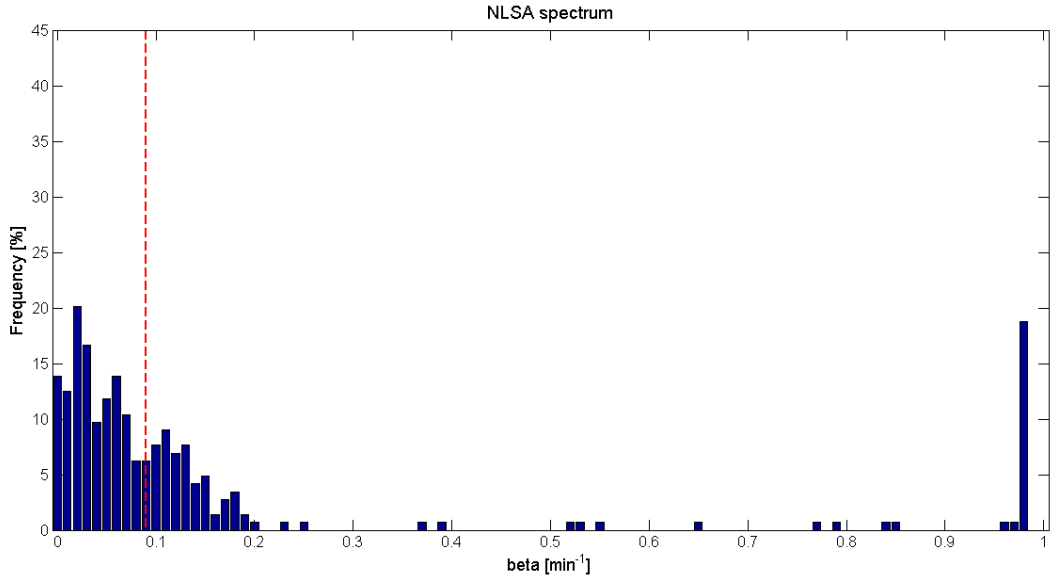

Figure 3.3: NLSA spectrum, possible cutoff = 0.09 $[min^{-1}]$.

A relative small number of boundary components is identified, 14% of ROIs contain a beta near zero while 24% have a beta in the $[0.98 : 0.99]$ $[min^{-1}]$ interval. These beta values are found when the two-exponentials model is unable to identified the slow or the fast component in the ROI thus one exponential hits the upper or the lower bound.

Furthermore, very slow exponentials, i.e. betas lower than 0.001 $[min^{-1}]$, suggest that the two-exponential model is collapsing to one-exponential with trapping component. As said in section 3.1, trapping component can be related to slow specific binding kinetics comparable with the length of PET exam. On the other hand, fast exponentials, that is betas higher than 0.9 $[min^{-1}]$, are associated with blood kinetics.

Comparing the various subjects, it is possible to study the inter-subject variability of the betas estimated. In the second and in the third subject a fast and a slow component are easily identified moreover few boundary betas are found. On the other hand, in the first and in the fourth, it is difficult to identify the fast one: several ROIs have a beta that hits the boundary value. For example, the test scan of the fourth subject has only 2 ROIs, Cerebellum and Thalamus, that contain a beta in [0.09:0.5] $[min^{-1}]$ interval.

LSA The spectrum obtained with LSA has different characteristics than NLSA (Figure 3.4):

- a higher number of boundary components is identified; in the 43% of the ROIs a beta lower than 0.01 $[min^{-1}]$ is found while 42% contain a beta higher than 0.99 $[min^{-1}]$.
- the separation between the two main components is clearer and a cutoff equal at 0.09 $[min^{-1}]$ can be derived.

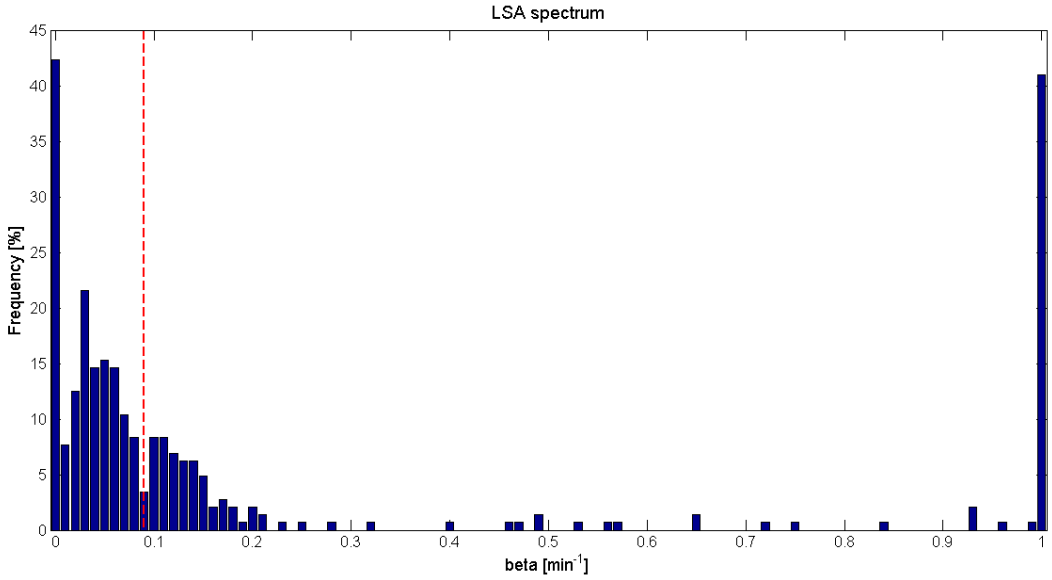

Figure 3.4: LSA spectrum, possible cutoff = 0.09 $[min^{-1}]$.

The presence of the boundary beta near 0 in the majority of the ROIs creates a significant difference in the beta values between LSA and NLSA. For example, in the Striatum of the second subject of the healthy data set the two main components calculated by LSA (in addition to that at 0.001) are equal at 0.046 and 0.145 $[min^{-1}]$ while with NLSA the two exponentials are identified in 0.019 and 0.135 $[min^{-1}]$. Thus, the beta near 0.001 $[min^{-1}]$ produces a shift of the main lines to higher frequencies.

On the other hand, betas higher than 0.95 $[min^{-1}]$ should be related to differences between the "true" arterial input function and that calculated and

used as input of the model. According to Cunnigham and colleagues, these high-frequency terms have relatively little effect on the size and position of lower-frequency components which relate to tissue retention and subsequent release of the tracer [17]. In this study, unnoticeable changes are caused by betas that hit the higher limit.

While the choice of the cutoff is not critical in NLSA since partial volumes of distribution can be obtained directly from the parameters of the single components, in the LSA it is a critical threshold. The ranges of betas related to the two main components have to be fixed in order to derive the partial volumes of distribution (Equation 2.19). Since LSA and NLSA give the same result, the β_{cutoff} is fixed at 0.09 $[min^{-1}]$. Therefore, the range of the slow component is [0.001 : 0.09] $[min^{-1}]$ while that relating to the fast component is fixed as [0.09:1] $[min^{-1}]$.

Considering the spectra, NLSA identifies a lower number of boundary components and does not need to define a cutoff value thus it is preferable to LSA.

3.4 Volume of distribution

Several ROIs obtained with NLSA are removed from the analysis due to non-reliable or non-physiological results (section 2.3.1): 6% in the test scan and 17% in the retest scan. The majority of them belongs to the fourth subject, respectively, the 75% and the 92%: this is caused by the lack of the fast component.

On the other hand, no ROI is removed in the LSA.

As regards LSA, in agreement with Myers and colleagues [12], the betas with values equal at the lower bound, i.e. 0.001 $[min^{-1}]$, are filtered, i.e. they are not used in the calculation of V_t and V_1, because they produce errors in the estimation of the parameters. The amplitude of the spectral lines at the lower bound is generally of the same order of magnitude of their betas thus their partial volumes, i.e. the ratio of amplitude over beta, are significant compared to the total volume of distribution. Furthermore, in particular ROIs such as Accumbens, the amplitude is an order higher than the beta and thus the resulting volume of distribution has non-physiological value. Then, components with frequency equal at the lower bound have to be filtered.

Instead, the boundary components at high frequencies have a little contribution to the volume of distribution since their amplitude is normally one or two orders of magnitude lower than their betas.

However, Myers and colleagues eliminate all the components greater than an estimated cutoff because they should relate to blood kinetics. This approach requires a second cutoff introducing more subjectivity therefore it is avoided.

NLSA For each ROI, the mean and the standard deviation of V_t, V_1 and V_5 between the four subjects in the test data-set obtained with NLSA are reported in Table 3.4.

ROI	V_t	SD	V_1	SD	V_5	SD
Whole Brain	3.89	0.51	1.52	0.95	2.38	1.37
Hippocampus	7.82	0.75	1.61	1.90	6.21	2.35
Amygdala	7.61	0.92	0.67	0.72	6.94	1.63
Cerebellum	2.24	0.24	2.24	0.24		
Insula	5.12	0.55	2.05	1.16	3.07	1.43
Caudate	3.94	0.56	1.41	1.08	2.53	1.61
Putamen	4.24	0.43	2.52	0.64	1.72	0.73
Striatum	4.19	0.42	2.52	0.72	1.66	0.82
Accumbens	9.04	0.41	1.17	2.09	7.87	2.47
Thalamus	2.74	0.20	1.05	0.87	1.69	0.98
Pallidum	4.46	1.86	1.87	0.55	2.59	1.31
Cingulate	5.89	0.58	1.54	2.10	4.74	2.21
Parietal lobe	3.70	0.49	0.91	1.34	2.79	1.67
Occipital lobe	3.90	0.52	1.03	1.44	2.87	1.76
Temporal lobe	4.96	0.58	0.91	1.33	4.04	1.76
Frontal lobe	4.07	0.44	0.90	1.36	3.17	1.72
Subcortical	4.89	0.48	2.28	0.64	2.60	0.67
Cortical	4.12	0.49	1.13	1.23	2.99	1.53
Mean	4.82	0.58	1.50	1.12	3.52	1.53
SD	1.76	0.36	0.61	0.51	1.86	0.53
SD%	36	62	40	45	53	35

Table 3.4: Between subject mean and variability (mean $\pm$ sd) of the volumes of distribution $[ml/cm^3]$ of the four subjects of the test data set obtained with NLSA.

The higher V_ts are found in Hippocampus, Amygdala, Accumbens and Cingulate in agreement with the known distribution of α_5 receptors. Moreover, the smallest V_ts are obtained in Cerebellum and Thalamus in which the amount of α_5 subunits is small.

In the majority of the ROIs, the between-subject SD is considerable (SD %>10%) due to the high inter-subject variability. In the pallidum the SD% is much higher (41%): the particular fit and the presence of trapping component discussed in previous section entail large difference between subjects. Accumbens is the region with lowest variability (SD%=5%).

As regards V_1 and V_5, according to [12] they should be related, respectively, with α_1 and α_5 receptors. However, the two exponential terms are not related to physiological compartments therefore some un-excepted results can be found:

- V_5 contributes most to the total volume of distribution.
- Hippocampus contains relative large amounts of α_1 subunit [1] but its V_1 is small compared to other ROIs such as Insula, Putamen and Striatum.

High variability between different ROIs is found in total and partial volumes of distribution due to the uneven distribution of GABA-A receptors.

LSA Similar results are obtained with LSA, reported in Table 3.5.

ROI	V_t	SD	V_1	SD	V_5	SD
Whole Brain	3.74	0.52	0.87	1.15	2.88	1.57
Hippocampus	7.32	0.73	0.56	0.85	6.76	1.27
Amygdala	7.02	1.35	0.88	0.44	6.58	1.62
Cerebellum	2.22	0.27	2.06	0.48	0.31	0.44
Insula	5.38	0.71	0.65	0.81	4.73	1.49
Caudate	3.93	0.58	0.76	0.90	3.17	1.33
Putamen	4.09	0.75	1.76	1.31	2.33	1.58
Striatum	4.07	0.72	0.93	1.08	3.14	1.69
Accumbens	8.16	1.29	0.28	0.15	8.01	1.25
Thalamus	2.64	0.27	1.05	0.72	1.59	0.85
Pallidum	3.23	2.66	0.68	0.82	2.55	3.13
Cingulate	5.88	0.58	1.53	2.11	4.73	2.21
Parietal lobe	3.59	0.61	1.15	1.38	2.72	1.77
Occipital lobe	3.89	0.52	1.38	1.55	2.85	1.75
Temporal lobe	4.90	0.62	1.24	1.47	3.96	1.75
Frontal lobe	4.02	0.48	1.19	1.48	3.12	1.75
Subcortical	4.94	1.07	0.83	0.94	4.11	1.96
Cortical	4.03	0.56	1.25	1.44	3.09	1.77
Mean	4.61	0.79	1.06	1.06	3.70	1.62
SD	1.60	0.55	0.44	0.48	1.90	0.55
SD%	35	69	42	45	51	34

Table 3.5: Between subject mean and variability (mean $\pm$ sd) of the volumes of distribution $[ml/cm^3]$ of the four subjects of the test data set obtained with LSA.

As seen in NLSA, Hippocampus, Amygdala, Accumbens and Cingulate have the highest V_t while the lowest are those of Cerebellum and Thalamus. Moreover, the between-subject variability in Pallidum is very high (SD% is equal to 83 %).

Partial volumes of distribution have more marked variations between the two methods. In LSA the V_1 is generally lower than NLSA, on average 30%,

while the V_5 is normally higher, on average 5%. Several factors contribute to this difference:

1. the filtering of the low boundary component,
2. the higher number of components in LSA, which produce difference in the beta values and thus in partial volumes of distribution.
3. the choice of the cutoff.

In the majority of the ROIs, high inter-subject variability is found with LSA, for example the SD%s of the whole brain are equal to 132% for V_1 and 55% for V_5. Most of the variability is due to the fourth subject.

Inconsistencies regarding the physiological informations reported with NLSA are still found with LSA, such as very low V_1 in Hippocampus.

Repeatability NLSA shows higher R^2 than LSA for V_t (Figure 3.5a and 3.5b). Also in terms of V_1 and V_5, NLSA outperformed LSA both in correlation (R^2) and repeatability (ICC), (Table 3.6).

Model	Parameter	V_t	V_1	V_5
LSA	R^2	0.71	0.53	0.76
	ICC	0.84	0.73	0.87
NLSA	R^2	0.93	0.70	0.91
	ICC	0.96	0.81	0.95

Table 3.6: Statistical index of NLSA and LSA

The cause of the lower R^2 in LSA is due to Pallidum; if they are not taken in account the R^2 is comparable to that obtained with NLSA. As reported in previous sections, Pallidum is a problematic region for both spectral methods. However, there are no reasons to exclude these values from the analysis (reliable and physiological estimates).

To note that V_1 has the lowest ICC and R^2, probably due to the lower contribution to V_t compared to V_5.

In terms of MRD, NLSA shows in general smaller MRD (Table 3.7). In agreement with previous results, V_1 has the highest variation between test and retest.

In light of all the results (goodness of fit, residuals, outliers, repeatability), NLSA is the method of choice in the base line dataset.

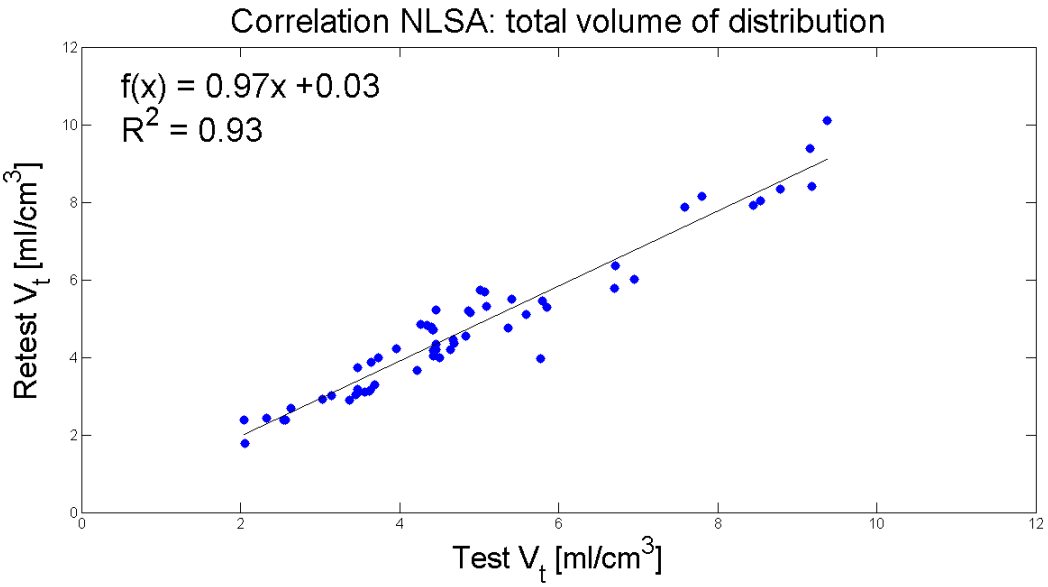

(a) Correlation between test-retest of NLSA.

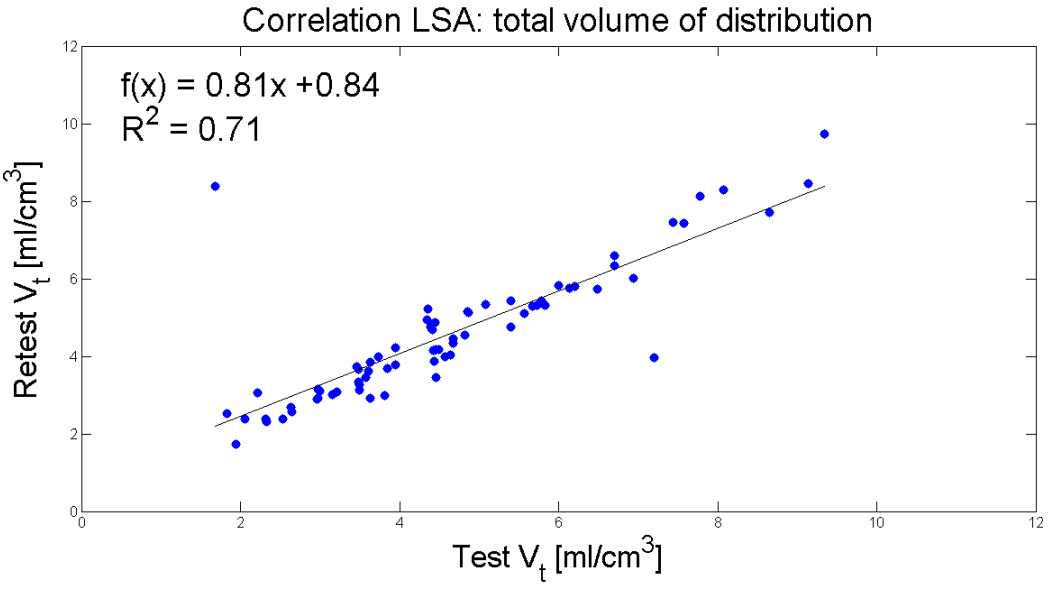

(b) Correlation between test-retest of LSA.

Figure 3.5: Correlation between test and retest scan.

	LSA		NLSA	
V_t	MRD	SD	MRD	SD
H1	11	13	8	8
H2	10	9	12	4
H3	7	7	6	3
H4	13	30	11	4
MEAN	10	15	9	4
SD	3	11	3	2
V_1				
H1	141	69	100	66
H2	30	52	18	24
H3	131	76	118	86
H4	106	73	59	96
MEAN	102	67	74	68
SD	50	11	45	32
V_5				
H1	38	53	16	12
H2	50	60	32	23
H3	38	60	21	15
H4	25	53	35	15
MEAN	38	57	26	16
SD	10	4	9	5

Table 3.7: Mean relative difference of V_t, V_1 and V_5 for each subject. Between subject mean and variability are reported.

3.5 Placebo-zolpidem data set

In the placebo-zolpidem data set, only one ROI obtained with NLSA (Amygdala of the third subject with placebo administration) is removed due to non-reliable result.

On the other hand, no ROI is removed in the LSA.

Whole brain results As regards V_t, little or no variations are found with NLSA while one subject shows an increment in the LSA in agreement with [12], (Figure 3.6a and 3.6d). Moreover, NLSA has a clearer reduction in V_1 compared to LSA where an increase of V_1 is reported after zolpidem administration (Figure 3.6b and 3.6e) in two subjects.

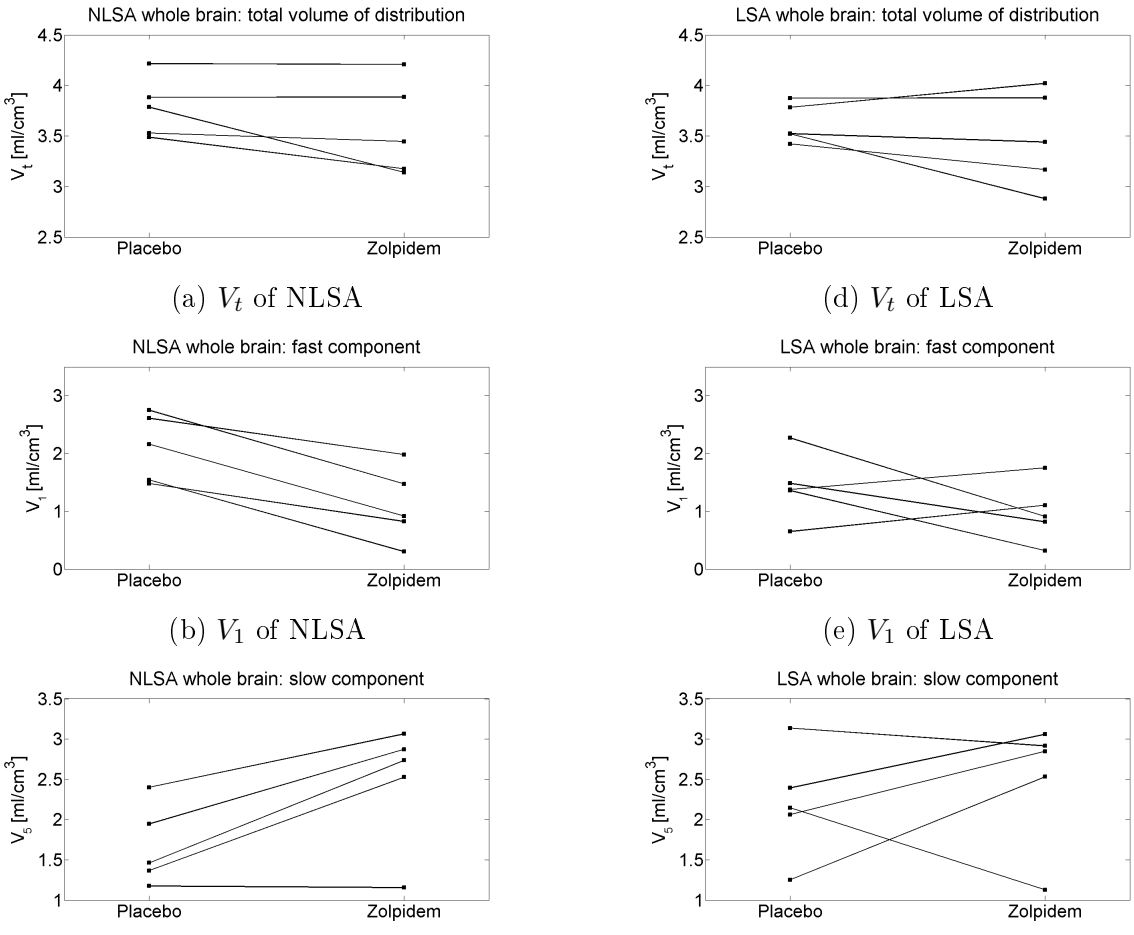

(a) V_t of NLSA

(d) V_t of LSA

(b) V_1 of NLSA

(e) V_1 of LSA

(c) V_5 of NLSA

(f) V_5 of LSA

Figure 3.6: Comparison of volumes of distribution between placebo and zolpidem obtained with NLSA and LSA

On the other hand, an increase of NLSA V_5 in four subjects is found (Figure 3.6c). Myers and colleagues do not report significant increases in the slow component however LSA produces plots less clear compared to NLSA (Figure 3.6f).

It is important to understand that the partial volumes calculated with spectral methods can not be matched with specific and non-displaceable (or non-specific) volumes of distribution because only with model-based quantification is possible to obtain them.

Regions of particular interest Between subject mean and SD of some representative regions are reported in Figure 3.7 and 3.8.

In each region, little or no decrease of V_t is found with both LSA and NLSA. The highest difference is reported in Accumbens (NLSA: PD=11%, LSA: PD=13%).

There is an overall decrease in V_1 obtained with NLSA and LSA after zolpidem administration. Furthermore, an increase of V_1 calculated with LSA is found in Hippocampus while with NLSA a little decrease is achieved. Moreover, a considerable difference is found in cerebellum by means of LSA in agreement with [12] (PD=22%).

In the majority of the ROIs there is an increase of V_5 obtained with NLSA. Instead, little or no increments are achieved with LSA in most regions, even though an increase is reported in whole brain (PD=-22%).

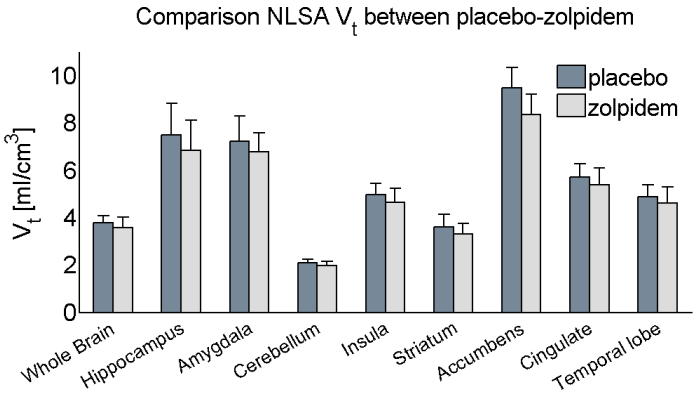

(a) Comparison of inter-subject mean and standard deviation of V_t between placebo-zolpidem.

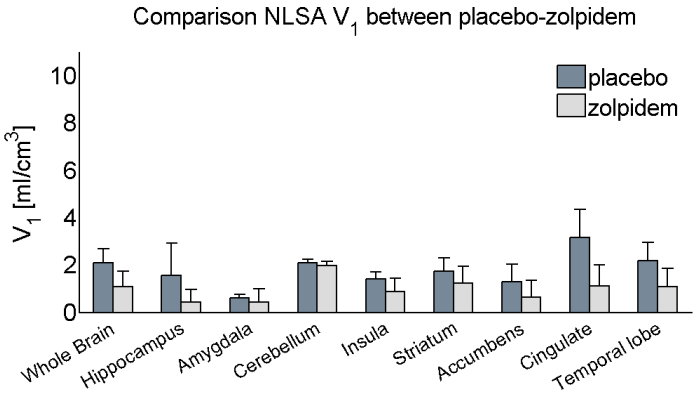

(b) Comparison of inter-subject mean and standard deviation of V_1 between placebo-zolpidem.

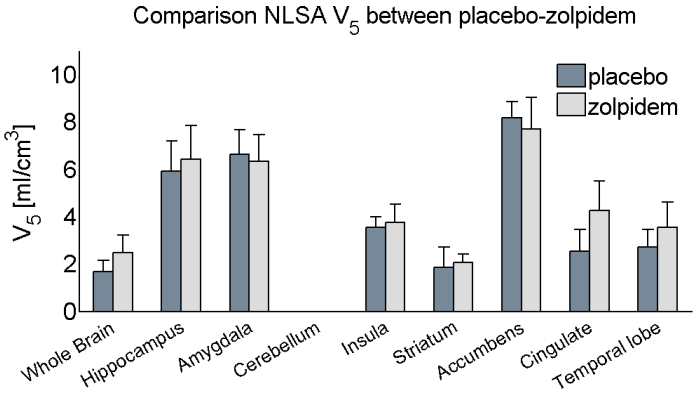

(c) Comparison of inter-subject mean and standard deviation of V_5 between placebo-zolpidem.

Figure 3.7: Mean and standard deviation between the fives subjects of partial and total volumes of distribution obtained with NLSA in placebo and zolpidem data set.

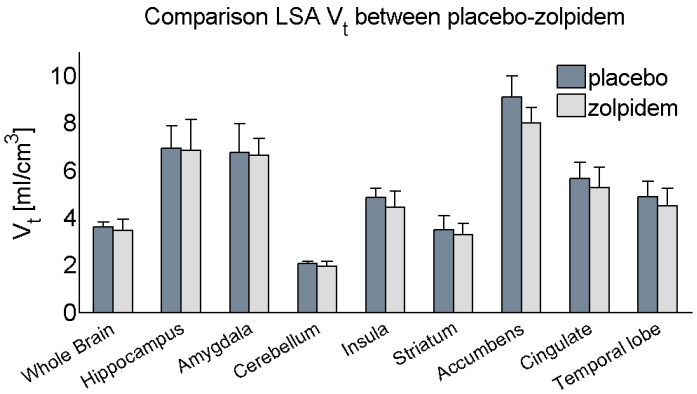

(a) Comparison of inter-subject mean and standard deviation of V_t between placebo-zolpidem.

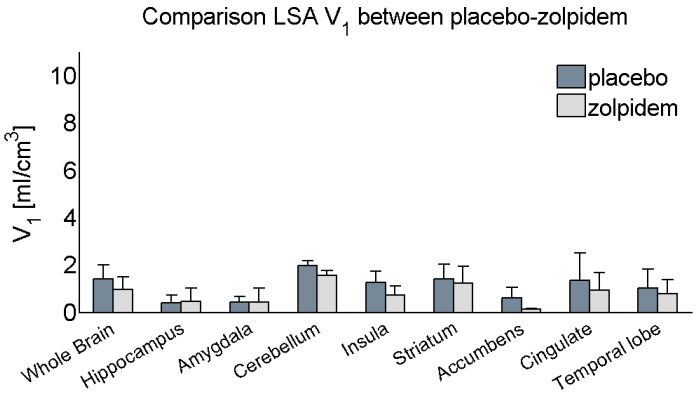

(b) Comparison of inter-subject mean and standard deviation of V_1 between placebo-zolpidem.

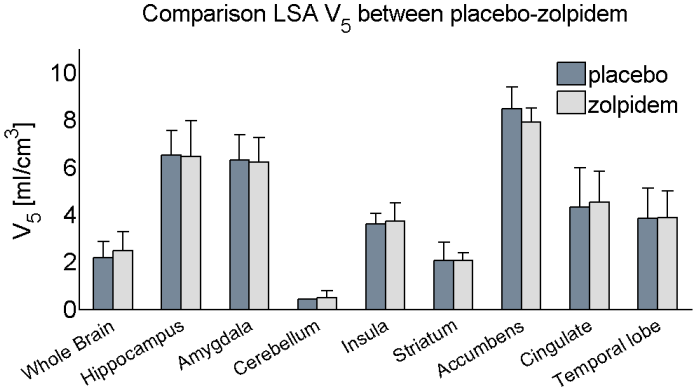

(c) Comparison of inter-subject mean and standard deviation of V_5 between placebo-zolpidem.

Figure 3.8: Mean and standard deviation between the fives subjects of partial and total volumes of distribution obtained with LSA in placebo and zolpidem data set.

3.6 Discussion and conclusion

Spectral methods are widely used in PET quantification since they need very few assumptions, they do not require any model structure and allow to calculate several macroparameters of interest.

In this study, non-linear spectral analysis and linear spectral analysis give reliable volume of distribution and identifies two main components: the slow one is likely related to GABA-A receptors containing α_5 subtype while the fastest is correlated with α_1 subtype given the decrease after zolpidem administration. In the Cerebellum in general only the fastest contribute is found (as expected since it does not contains α_5 receptors).

In general NLSA outperforms LSA as it:

- avoids the overestimation of the number of components (in particular a reduced percentage of boundary betas are found).
- better fits the time activity curves of the in all the ROIs and random and uncorrelated weighted residuals are achieved (which are highly correlated in LSA). Furthermore, the quality of the fits and the weighted residuals of the LSA are grid-dependent.
- does not need the definition of a cutoff value to calculate partial volumes of distribution.
- has higher repeatability (test-retest dataset).

On the other hand, LSA is more flexible, since the number of components is not fixed a priori resulting in a smaller percentage of outliers. Furthermore, it is computationally faster than NLSA.

Through the placebo-zolpidem data set, confirmations on the relation between fast component and α_1 receptors were found. Moreover, overall increment in the slow component is reported and it could be caused by the higher bioavailability of the tracer in the extra-synaptic space.

Finally, a better separation of the partial volumes of distribution is achieved with NLSA since similar behaviour are found between the different subjects in the placebo-zolpidem data set.

Model-based quantification is now needed to study the physiological interpretation of the tracer such as specific and non-specific binding.

Chapter 4

Quantification results: model-driven methods

In the in-vivo receptor studies 2-TCM is widely used: the tissue TAC is described by the sum of the free plus non-specifically bound and the specifically bound ligand. This model is a simplification of the general model containing three compartments (3-TCM) that further divides the free and the non-specific binding kinetics [21].

In the 13% of the ROIs 3-exponential terms are found by NLSA and thus three tissue compartments may be identified. In some representative subjects with high frequency of these ROIs, the 3-TCM is used to describe [^{11}C]Ro15-4513 data and the results are compared with 2-TCM data description.

4.1 Comparison 3-TCM and 2-TCM

The structure of the 3-TCM is reported in Figure 4.1.

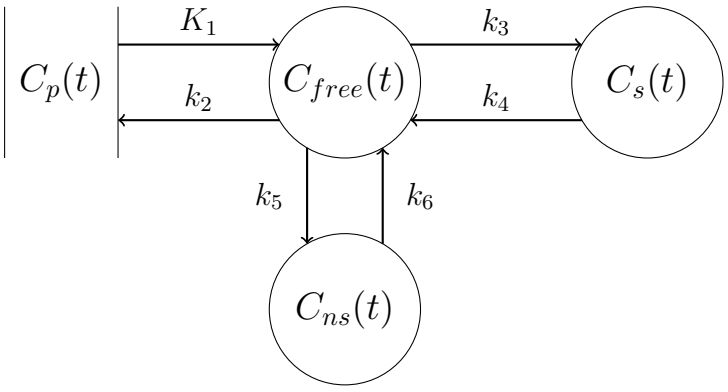

Figure 4.1: Three tissue compartment model

where $C_{free}(t)$ is the concentration of free tracer, $C_{ns}(t)$ is the concentration of non-specifically bound tracer while $C_s(t)$ is related to the specific binding.

Generally, a tracer is specific for only one receptor, instead the [^{11}C]Ro15-4513 has significant affinities to several α subtypes (Table 2.1). Since the tracer has an affinity 5-10 fold higher for α_5 subtype than for the others, it is bound with high specificity and thus its binding kinetics is slow. The [^{11}C]Ro15-4513 binding to the other subtypes has low specificity thus the resulting kinetics are fast phenomena comparable to the non-specific binding.

Therefore, the $C_s(t)$ could be related to α_5 subtype while the $C_{ns}(t)$ should contain the non-specific binding and the GABA-A receptors with low affinity, i.e. α_1, α_2, α_3, α_4 and α_6.

Total and partial volumes of distribution can be calculated from the kinetic parameters in similar way as 2-TCM. They are given by:

$$V_t = \frac{K_1}{k_2}(1 + \frac{k_3}{k_4} + \frac{k_5}{k_6}) \tag{4.1}$$

$$V_{free} = \frac{K_1}{k_2} \tag{4.2}$$

$$V_s = \frac{K_1 k_3}{k_2 k_4} \tag{4.3}$$

$$V_{ns} = \frac{K_1 k_5}{k_2 k_6} \tag{4.4}$$

In three subjects of interest, the kinetics of the compartments and the inter-subject mean of V_s (it will be called V_5) are compared to those obtained with 2-TCM (in the same subjects) in order to study their relationship.

Fit and compartments In Figure 4.2 and 4.3, model descriptions and the kinetics of the single compartments are reported for the Hippocampus of the second subject of the healthy dataset, described by 3-TCM and 2-TCM respectively.

The kinetics of the specific compartment almost does not change from 3-TCM to 2-TCM. In any case, in the majority of the regions, the 2-TCM can not separate the non-specifically bound tracer from the free because they have both fast kinetics.

Assuming therefore that the specific binding of 2-TCM is related to α_5 binding, then the concentration of the first compartment obtained with 2-TCM is related to three main components:

1. free tracer,
2. non-specific binding,
3. GABA-A receptors containing α_1, α_2, α_3, α_4 or α_6 subunit.

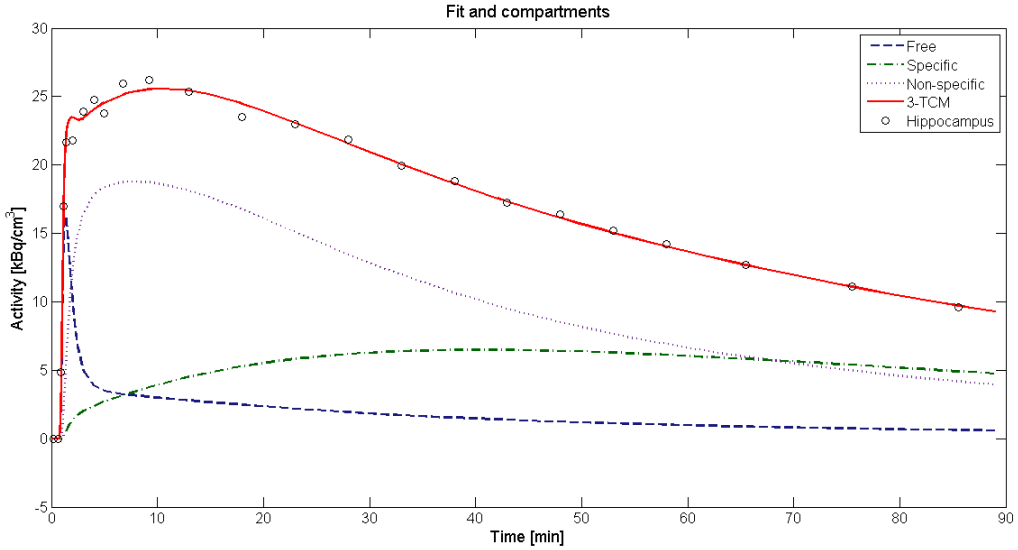

Figure 4.2: Fit and kinetics of the compartments by 3-TCM.

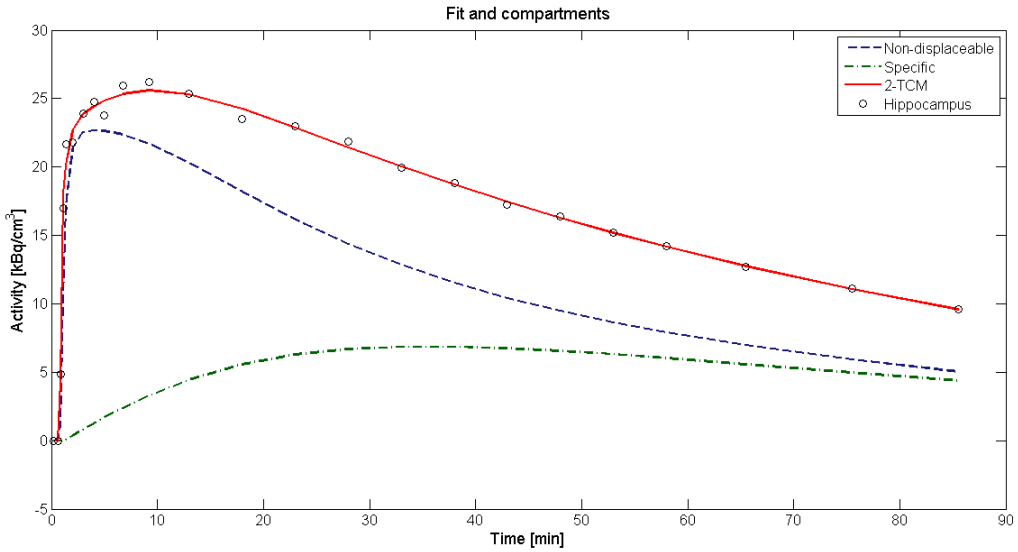

Figure 4.3: Fit and kinetics of the compartments by 2-TCM.

In order to verify the equality of the specific compartments achieved with the different models, the V_5s averaged among the three subjects are compared (Figure 4.4).

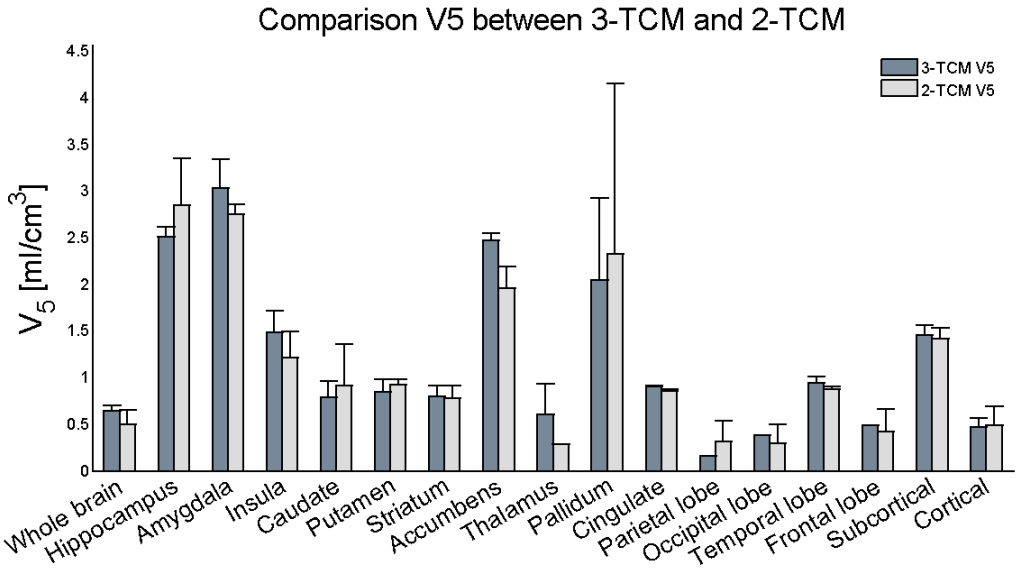

Figure 4.4: Comparison of the V_5s obtained with 3-TCM and 2-TCM.

Overall, little or no variation on V_5 is found in the majority of the ROIs. As seen in the previous chapter, the Pallidum has very high inter-subject variability.

The differences in the kinetic parameters obtained with 3-TCM and 2-TCM are calculated: the main change is found in k_2 (PD=30%) while K_1, k_3 and k_4 have small variations.

Therefore, the distribution of the α_5 receptors can be determined from the V_5, i.e. the volume of distribution of the second compartment, of the 2-TCM.

4.2 Quantification results of 2-TCM

In the Section 2.2.5, the similarity between the concentrations of the tissue obtained with 2-TCM and 2-exponentials NLSA was discussed: both methods describe the TAC with two exponential terms and no major differences are expected on goodness of fit and total V_t. On the contrary, there is no direct correspondence between single components and model compartments.

4.2.1 Fit and weighted residual

In the Figure 4.5, 2-TCM fit, weighted residuals and the tracer concentrations of the two compartments are reported for the Insula region for one representative subject.

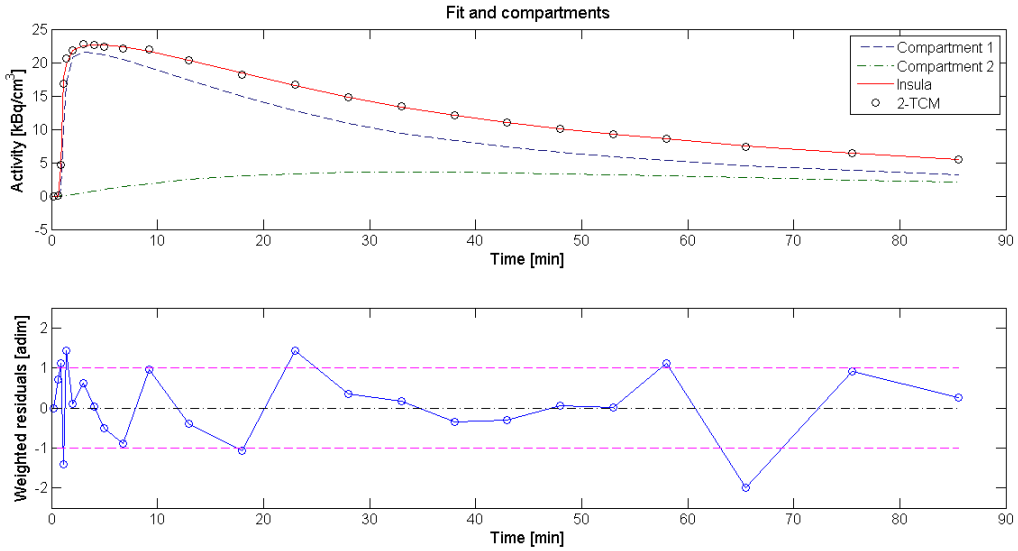

Figure 4.5: Fits, weighted residuals and kinetics of the compartments of Insula by 2-TCM.

As excepted, 2-TCM fit and weighted residuals are almost identical to those of NLSA (Figure 3.1), few differences are due to the approximations in the estimation caused by the numerical solution of the differential equations.

The curves related to the two compartments are instead significantly different: the concentration of the first compartment of NLSA is usually lower compared to that obtained with 2-TCM, while the second one is usually higher.

4.2.2 Volumes of distribution

The number of non-reliable and non-physiological ROIs is equal to that reported in section 3.4.

The mean and the standard deviation of V_t, V_1 and V_5 across the four subjects in the test data set are reported for each ROI in Table 4.1.

To note that as regards V_t, no differences (on average $<0.002\%$) are found between 2-TCM and NLSA (Table 3.4) in agreement with previous considerations. Moreover, same inter-subject and inter-ROI variability are achieved.

For 2-TCM the greatest contribution to the V_t is given by V_1 (instead of V_5 as with the NLSA). On average, 76% of V_t is due to V_1 while 24% by V_5.

The highest V_5s are found in Hippocampus, Amygdala and Accumbens in agreement with the distribution of α_5 receptors. Afterwards, the lowest ones are found in Parietal lobe and Occipital lobe in which only few GABA-A receptors contain α_5 subtype. In general, a less between-subject variability in V_5 compared to NLSA is obtained (for example in whole brain 2-TCM

SD%=34 while NLSA SD%=58), however a higher variability between the ROIs is present due to the uneven distribution of the α_5 subtype (on average 2-TCM SD%=79, NLSA SD%=53).

The Pallidum remains a particular region: a high V_5 is found even if high expression of α_5 is not reported in studies concerning the GABA-A receptor complex.

As regards V_1, it is important to recall that it does not directly describe the α_1 receptors since free tracer, non-specific binding and GABA-A receptors containing α_2, α_3, α_4, and α_6 subtype contribute to the kinetics of the first compartment. Thus, the interpretation of the V_1 results complex.

However, some interesting observations can be made:

- the highest values are found in the limbic area, i.e. Hippocampus, Amygdala and Accumbens, in which good amounts of GABA-A receptors are found, in particular α_2 and α_3.
- the lowest values are found in Cerebellum and Thalamus which do not contain high level of α_5, but α_1, α_4 and α_6.

These observations are, obviously, qualitative since the free tracer and the non-specific receptors are also included in V_1, even if their contribution should be equal in each regions.

Repeatability As excepted, very similar results to NLSA for V_t are found (Figure 4.6).

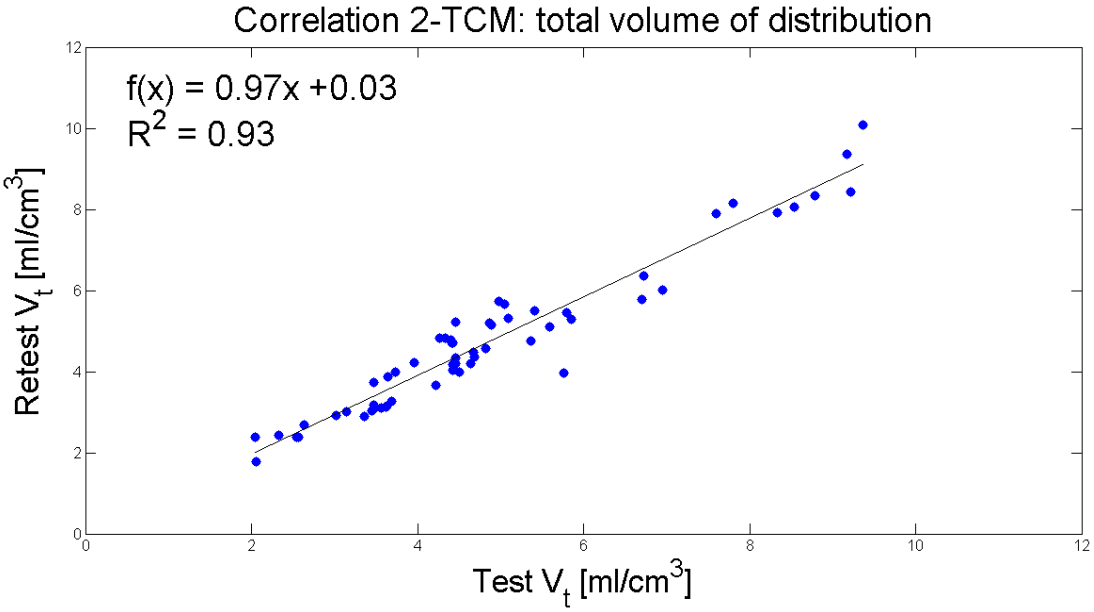

Figure 4.6: Correlation between test-retest of 2-TCM.

2-TCM instead performed differently as regards V_1 and V_5 (Table 4.2).
Overall, lower values are found with the 2-TCM compared to the NLSA.

ROI	V_t	SD	V_1	SD	V_5	SD
Whole Brain	3.89	0.51	3.28	0.65	0.62	0.21
Hippocampus	7.72	0.79	4.47	0.55	3.25	0.52
Amygdala	7.61	0.92	5.19	1.39	2.42	0.52
Cerebellum	2.24	0.24	2.24	0.24		
Insula	5.11	0.56	3.93	0.78	1.17	0.51
Caudate	3.94	0.56	3.14	0.66	0.80	0.35
Putamen	4.24	0.43	3.29	0.49	0.94	0.26
Striatum	4.18	0.42	3.30	0.46	0.88	0.29
Accumbens	9.02	0.47	5.87	0.89	3.15	1.23
Thalamus	2.73	0.20	2.08	0.46	0.65	0.42
Pallidum	4.45	1.85	2.45	0.70	1.99	1.14
Cingulate	5.89	0.58	5.24	1.02	0.66	0.47
Parietal lobe	3.70	0.49	3.39	0.62	0.31	0.22
Occipital lobe	3.90	0.52	3.61	0.63	0.29	0.20
Temporal lobe	4.96	0.58	4.12	0.66	0.84	0.18
Frontal lobe	4.07	0.44	3.65	0.60	0.42	0.25
Subcortical	4.88	0.48	3.41	0.52	1.47	0.25
Cortical	4.12	0.49	3.63	0.60	0.48	0.21
MEAN	4.82	0.59	3.68	0.66	1.20	0.43
SD	1.75	0.36	1.01	0.25	0.95	0.31
SD%	36	61	27	38	79	73

Table 4.1: Mean and standard deviation of volumes of distribution across the four subjects of the test data set obtained with 2-TCM.

Model	Parameter	V_t	V_1	V_5
2-TCM	R^2	0.93	0.64	0.50
	ICC	0.97	0.79	0.66

Table 4.2: Statistical indexes of 2-TCM

In particular, the first and the fourth subject, which have poor repeatability and some problems in the estimation for all models, influence significantly the robustness of the 2-TCM. In fact, the R^2 and the ICC of V_5 in the second subject, which is the best one for all models, are, respectively, 0.89 and 0.90.

Moreover, V_1 has a better R^2 and ICC than V_5 due to the greater contribution to the V_t.

As regards MRD, 2-TCM V_t results are similar to those obtained with NLSA (Table 4.3).

V_t	MRD	SD	V_1	MRD	SD	V_5	MRD	SD
H1	8	8		14	13		44	36
H2	12	4		7	4		43	25
H3	6	3		23	9		78	52
H4	11	4		3	5		70	23
MEAN	9	4		12	8		59	34
SD	3	2		9	4		18	13

Table 4.3: Mean relative difference of V_t, V_1 and V_5 with 2-TCM for each subject. Between subject mean and variability are reported.

On the other hand, better values are found by 2-TCM for V_1 compared to NLSA while smaller repeatability is achieved for V_5. These difference are due to the different contributions of the partial volumes of distribution in the different models: in the NLSA the greatest contribute is given by V_5 while in the 2-TCM it is given by V_1.

Overall, good MRDs are found for V_t and V_1 while notable variations for V_5 are reported.

4.2.3 Placebo-zolpidem data set

As reported in section 3.5, the Amygdala of the third subject is removed due to non-reliable and non-physiological estimates.

Whole brain results As regards the whole brain of the five subjects, similar results to NLSA are achieved (Figure 4.7):

- little or no variations are found in V_t for all the five subjects,
- there's a clearer reduction in V_1 after zolpidem administration due to the blocking of the α_1 receptors,
- instead, an increase in V_5 is reported.

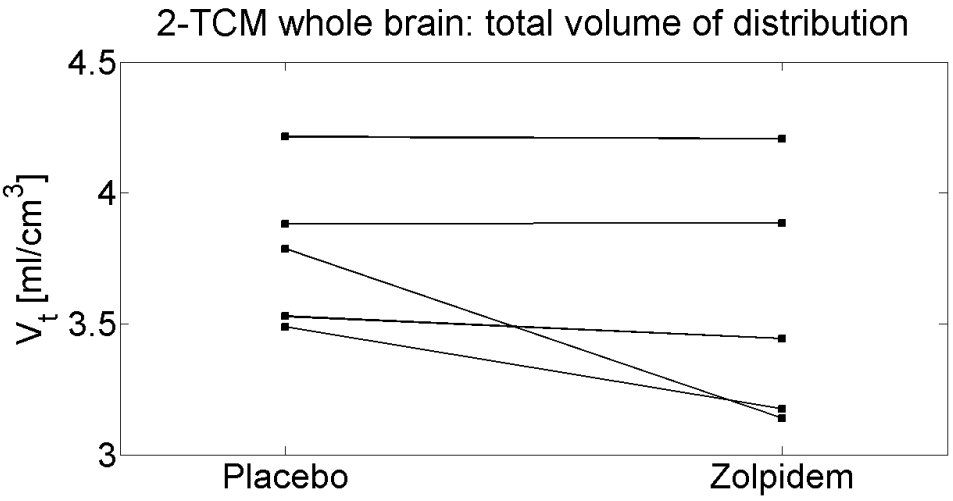

(a) V_t of whole brain in the five subjects.

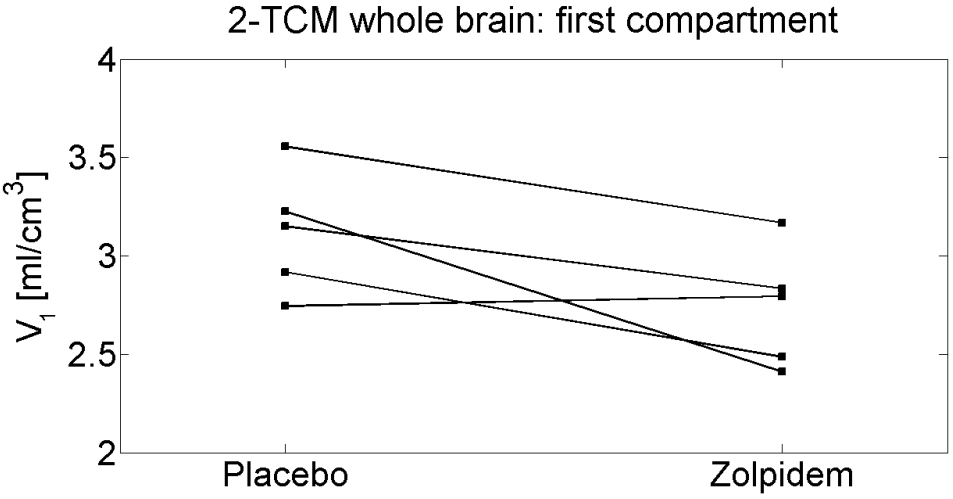

(b) V_1 of whole brain in the five subjects.

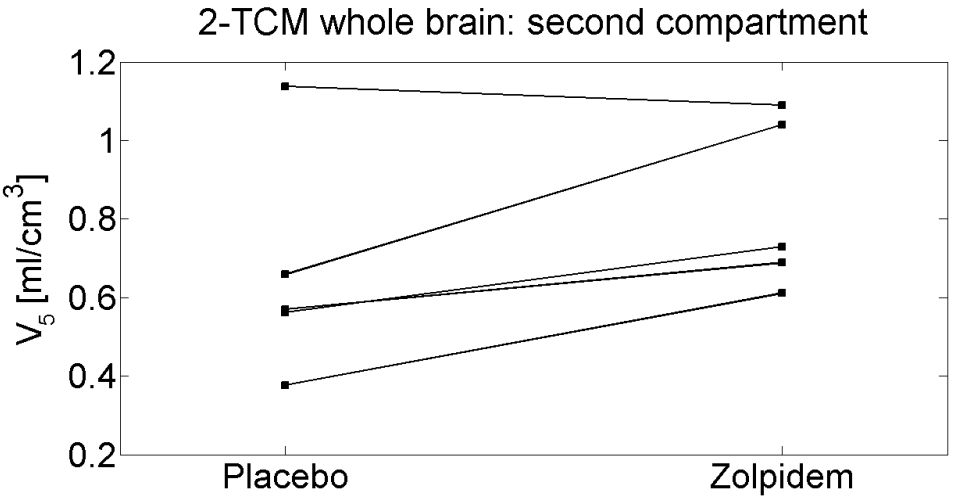

(c) V_5 of whole brain in the five subjects.

Figure 4.7: Comparison of volumes of distribution between placebo and zolpidem obtained with 2-TCM.

A possible explanation is proposed to describe the increase of V_5.

The rate constants for transfer between the specific and the non-displaceable compartment, i.e. k_3 and k_4 are defined as:

$$k_3 = k_{on} f_{ND} B_{MAX} \tag{4.5}$$

$$k_4 = k_{off} \tag{4.6}$$

where

- k_{on} is the rate constant of association between the ligand, i.e. the tracer, and the specific receptor,
- k_{off} is the rate constant of dissociation of the tracer-receptor complex,
- f_{ND} is the fraction of free tracer in the non-displaceable compartment,
- B_{MAX} is the number of specific receptors available to binding.

In standard receptor studies, the non-displaceable compartment contains only the free and the non-specifically bound tracer thus f_{ND} is given by:

$$f_{ND} = \frac{V_{free}}{V_{free} + V_{ns}} \tag{4.7}$$

where V_{free} is the volume of the free tracer while V_{ns} is the volume related to the non-specific binding.

As seen in the initial part of this chapter, with [^{11}C]Ro15-4513 the first compartment also contains the low-specific GABA-A receptors therefore f_{ND} is formulated as:

$$f_{ND} = \frac{V_{free}}{V_{free} + V_{ns} + V_{\alpha_1} + V_{\alpha_2} + V_{\alpha_3} + V_{\alpha_4} + V_{\alpha_6}} \tag{4.8}$$

Defining OCC as the occupancy of the α_1 receptors after the zolpidem, the f_{ND} after the administration of the drug can be written as:

$$f_{ND}^{zolpidem} = \frac{V_{free}}{V_{free} + V_{ns} + (1 - OCC)V_{\alpha_1} + V_{\alpha_2} + V_{\alpha_3} + V_{\alpha_4} + V_{\alpha_6}} \tag{4.9}$$

where $0 \leq OCC \leq 1$ and therefore $f_{ND}^{zolpidem} \geq f_{ND}$.

Consequently, $k_3^{zolpidem} = k_{on} f_{ND}^{zolpidem} B_{MAX} \geq k_3$.

Therefore, the V_5 obtained with 2-TCM, i.e. the specific binding of α_5, also increases while V_1 decreases due to the lower V_{α_1}.

Regions of particular interest Figure 4.8 reports between subject mean and variation of V_t, V_1, V_5 of the five subjects after placebo and zolpidem administration in some representative regions.

In agreement with the considerations just made, little or no variations are found in V_t while larger differences are reported in V_1. On the other hand, there's an increase in V_5 in each ROI taken in consideration. The Cerebellum is described by 1-TCM therefore no V_5 is present.

As seen with the NLSA, the highest percentage differences in V_t and V_1 between placebo and zolpidem administration are found in Accumbens (V_t: 12%, V_1: 28%). Furthermore, Hippocampus (V_t: 8%, V_1: 24%) and Amygdala (V_t: 5%, V_1: 21%) show notable reductions. On the other hand, the lowest are reported in Whole Brain (V_t: 6%, V_1: 12%) and Cerebellum (V_t: 6%, V_1: 6%).

The small variation in the Cerebellum may be due to the presence of the α_6 subtype which is insensitive to zolpidem [3] [4].

As regards V_5, notable increases (PD $<$ -15 %) are found in the majority of the ROIs. The lowest increase is found in the Insula (PD = -7%).

Furthermore, high increases are reported in lobe areas: Parietal lobe (PD=-38%), Occipital lobe (PD=-59%) and Frontal lobe (PD=-35%). These areas contain high amounts of α_1 receptors and thus there is a high decrease of the V_{α_1} due to zolpidem administration. Consequently, a notable increase of $k_3^{zolpidem}$ is obtained due to the increase of $f_{ND}^{zolpidem}$ (Equation 4.9). Therefore, an higher V_5 is produced.

Considering all results, the 2-TCM is the suggested model for the quantification of [^{11}C]Ro15-4513 PET data at ROI level since its V_5 is related to GABA-A receptors containing α_5 subtype. Instead, the NLSA V_5 is a "mixture" of model compartments and thus it can not be used to evaluate the distribution of α_5 receptors.

Furthermore, it is not possible to obtain the density of α_1 receptors because the non-displaceable compartment contains several contributions.

4.3 Genomic integration

In [29], it was demonstrated that brainwide mRNA mapping may be highly predictive of in vivo protein levels.

As regards GABA-A receptor complex, no previous studies have compared the mRNA expression data obtained from Allen Human Brain Atlas and the parameters of interest obtained with PET images.

In this section, the Spearman's correlations between PET results and mRNA levels will be reported to assess the correlations between their spatial distribu-

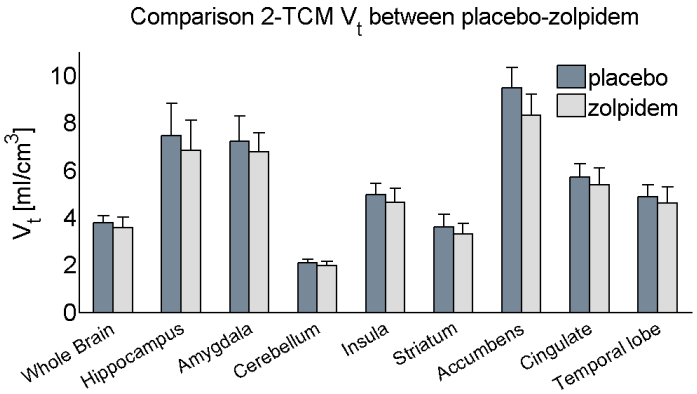

(a) Comparison of the inter-subject mean and the standard deviation of V_t between placebo-zolpidem.

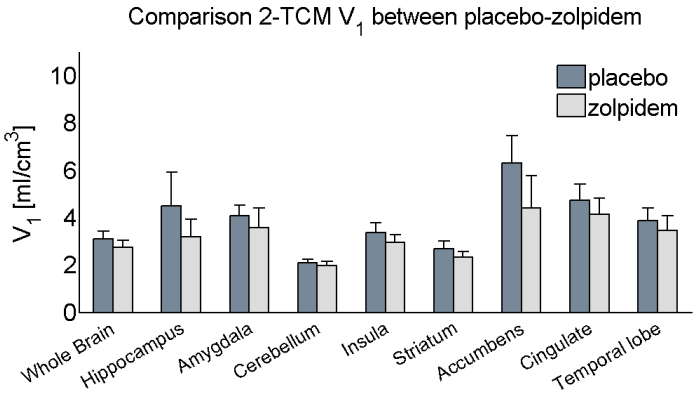

(b) Comparison of the inter-subject mean and the standard deviation of V_1 between placebo-zolpidem.

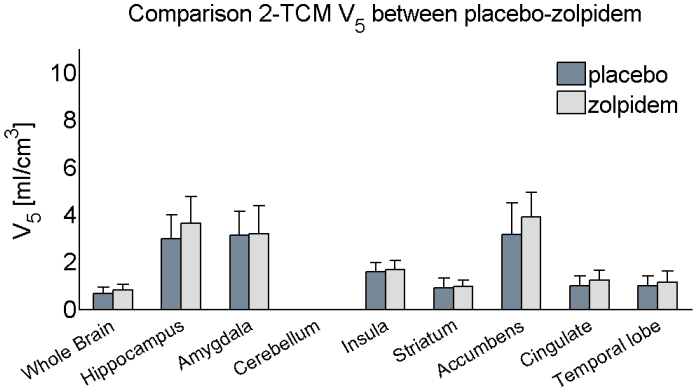

(c) Comparison of the inter-subject mean and the standard deviation of V_5 between placebo-zolpidem.

Figure 4.8: Inter-subject mean and inter-subject standard deviation of partial and total volumes of distribution obtained with 2-TCM in placebo and zolpidem data set.

tion.

4.3.1 mRNA data

For each α subtype, the level of GABA mRNA expression (GABRA) is calculated for several ROIs, see Appendix A.4. The Pallidum is removed from the analysis as confounding factor.

As regards GABRA5, i.e. the gene related to α_5 subunit, its expression is in agreement with the physiological information described in several studies: the highest values are found in Hippocampus and Amygdala while the lowest one in Cerebellum. Furthermore, medium levels of expression are reported in Insula, Striatum, Cingulate gyrus and Temporal lobe.

Also the expressions of the other GABRA genes are in agreement with the distributions of the respective subtypes. For example, high GABRA1 and GABRA6 values are found in the Cerebellum.

However, it is necessary to take in consideration that several factors can influence the relationship between the measurements of mRNA and the expression of the respective subtypes such as posttranscriptional changes. Thus, with the levels of mRNA, it is possible to obtain only "semi-quantitative" informations.

The distributions of the different GABRA mRNA levels are compared to study their spatial correlations (Table 4.4).

	GABRA1	GABRA2	GABRA3	GABRA4	GABRA5	GABRA6
GABRA1	1.00	-0.62	-0.35	-0.35	-0.62	0.89
GABRA2	-0.62	1.00	0.68	0.55	0.98	-0.35
GABRA3	-0.35	0.68	1.00	0.06	0.69	-0.28
GABRA4	-0.35	0.55	0.06	1.00	0.53	-0.21
GABRA5	-0.62	0.98	0.69	0.53	1.00	-0.37
GABRA6	0.89	-0.35	-0.28	-0.21	-0.37	1.00

Table 4.4: Spearman's ρ between all GABRA genes.

A high spatial correlation is found between GABRA2 and GABRA5 and a notable one between GABRA3 and GABRA5. Furthermore, a significant ρ is achieved between GABRA1 and GABRA5 albeit negative.
On the other hand, GABRA4 and GABRA6 are poorly correlated with GABRA5.

The similar spatial distribution of α_2, α_3 and α_5 makes the statistical analysis complicated since it can produce indirect correlations between the distributions of their GABRA genes and the volumes of distribution obtained with the mathematical models.

4.3.2 Correlations between GABRA and volumes of distribution

For each GABRA gene, the averages of V_t, V_1 and V_5 across the four subjects of the test data set are compared to the mRNA expression. In Figures 4.9-4.11, the ROIs are ordered according to increasing values of GABRA expression: ROIs with lower expressions are on the left side while ROIs with higher values of mRNA are on the right side of the x-axis.

Thus, if a particular volume of distribution is highly correlated to a specific GABRA gene, an increase of its value from left to right of the graph should be seen.

Total volume of distribution In Figure 4.9, V_t values obtained with 2-TCM and NLSA are reported for GABRA1 and GABRA5. Comparison for GABRA1,3,4 and 6 are reported in Appendix B.

ρ^2s values are reported in Table 4.5.

		GABRA1	GABRA2	GABRA3	GABRA4	GABRA5	GABRA6
V_t	NLSA	0.27	0.84	0.67	0.21	0.89	0.13
	2-TCM	0.27	0.84	0.67	0.21	0.89	0.13
V_1	NLSA	0.03	0.00	0.15	0.03	0.00	0.00
	2-TCM	0.04	0.50	0.73	0.10	0.53	0.02
V_5	NLSA	0.00	0.37	0.84	0.01	0.37	0.00
	2-TCM	0.50	0.84	0.45	0.04	0.84	0.15

Table 4.5: Spearman's ρ^2 between the volumes of distribution, obtained with 2-TCM and NLSA, and the distributions of GABRA.

As discussed in previous sections, the V_ts obtained with NLSA and 2-TCM are almost equal (Figure 4.9). Furthermore, there is a high correlation between V_t and GABRA5 probably due to the high affinity of the tracer for the GABA-A receptors containing α_5 subunit.

No significant ρ^2 are achieved for GABRA1, GABRA4 and GABRA6.

Notable correlations between V_t and GABRA2 and GABRA3 are found due to the high correlation in the spatial distribution between GABRA5 and GABRA2,3(Table 4.4).

Partial volumes of distribution 2-TCM V_5 shows high correlation with GABRA5 mRNA leves (and also GABRA2, due to the high genomic autocorrelation) compared to NLSA V_5.

This finding supports the hypothesis that NLSA components describe a "mixture" of model compartments.

Both NLSA and 2-TCM V_1 do not show any correlation with GABRA, expect 2-TCM V_1 with GABRA3 (Table 4.5).

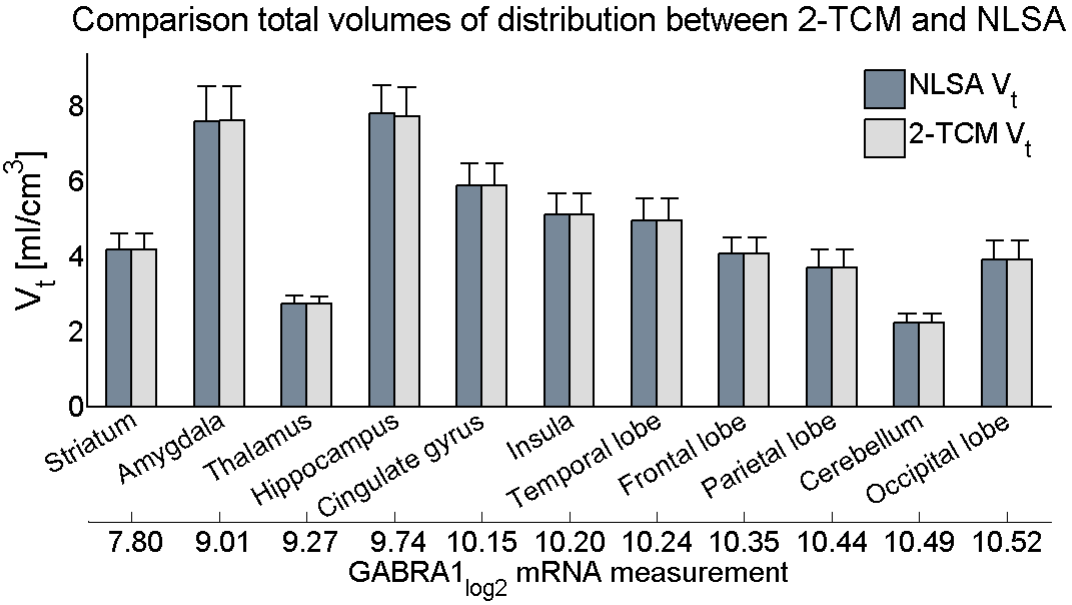

(a) Order of the ROIs due to GABRA1 expression.

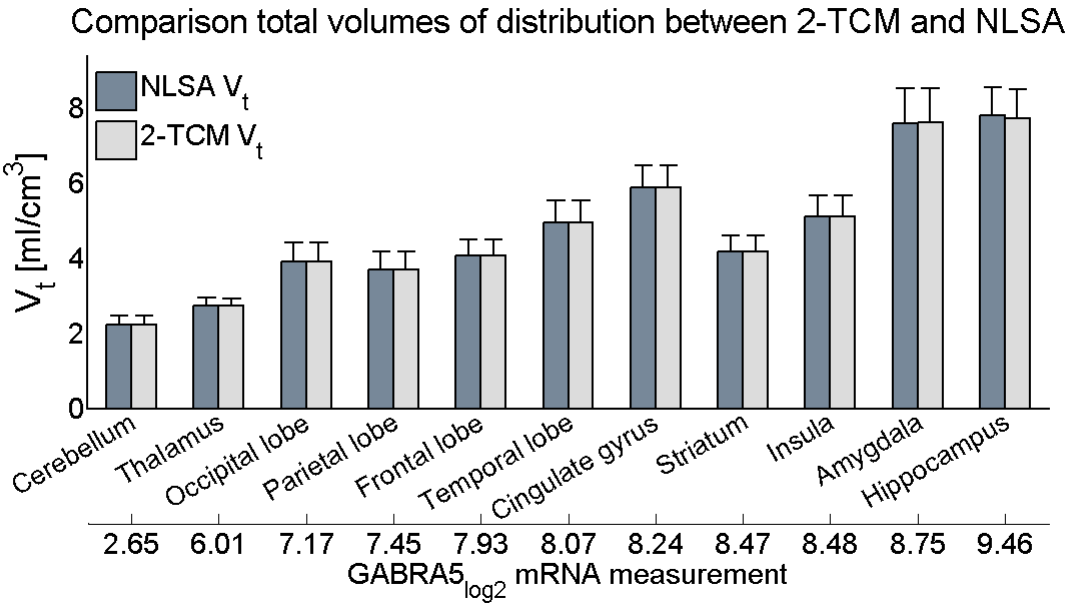

(b) Order of the ROIs due to GABRA5 expression.

Figure 4.9: Comparison of V_t sorted according to the expressions of the GABA genes.

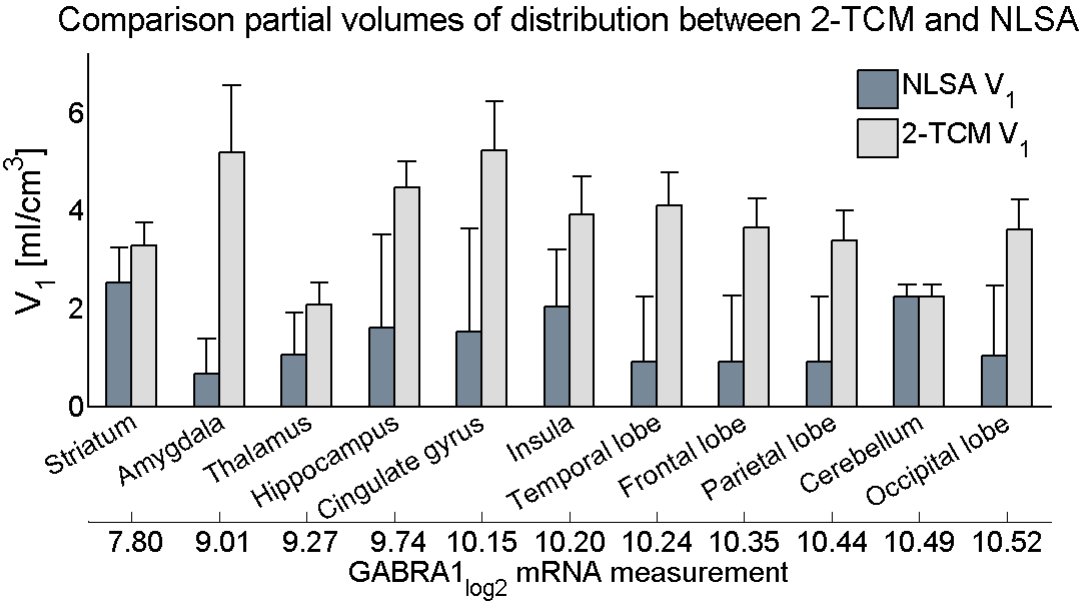

(a) Order of the ROIs due to GABRA1 expression.

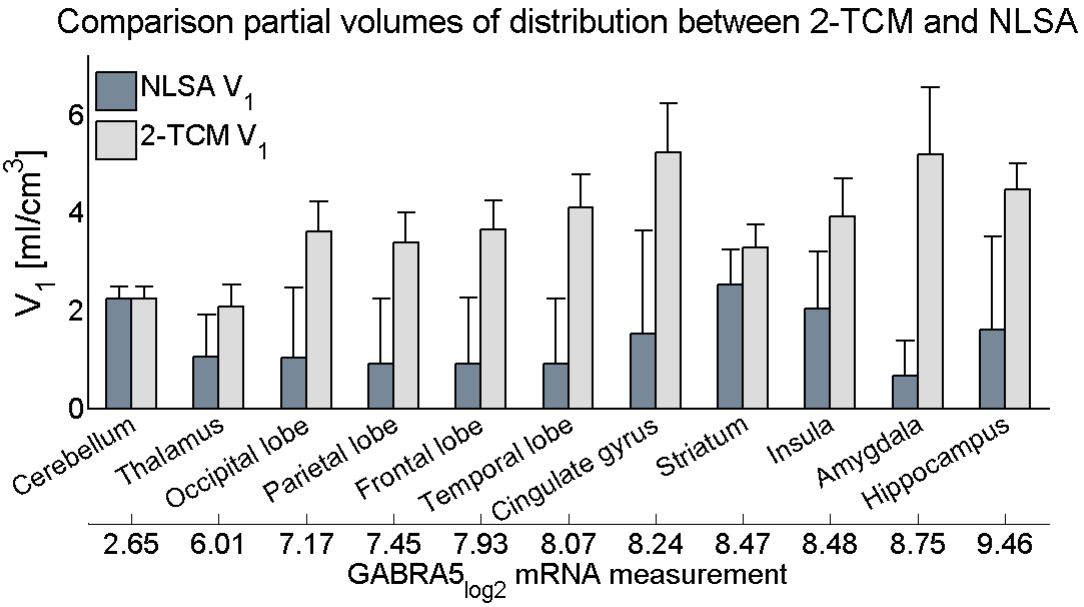

(b) Order of the ROIs due to GABRA5 expression.

Figure 4.10: Comparison of V_1 sorted according to the expressions of the GABA genes.

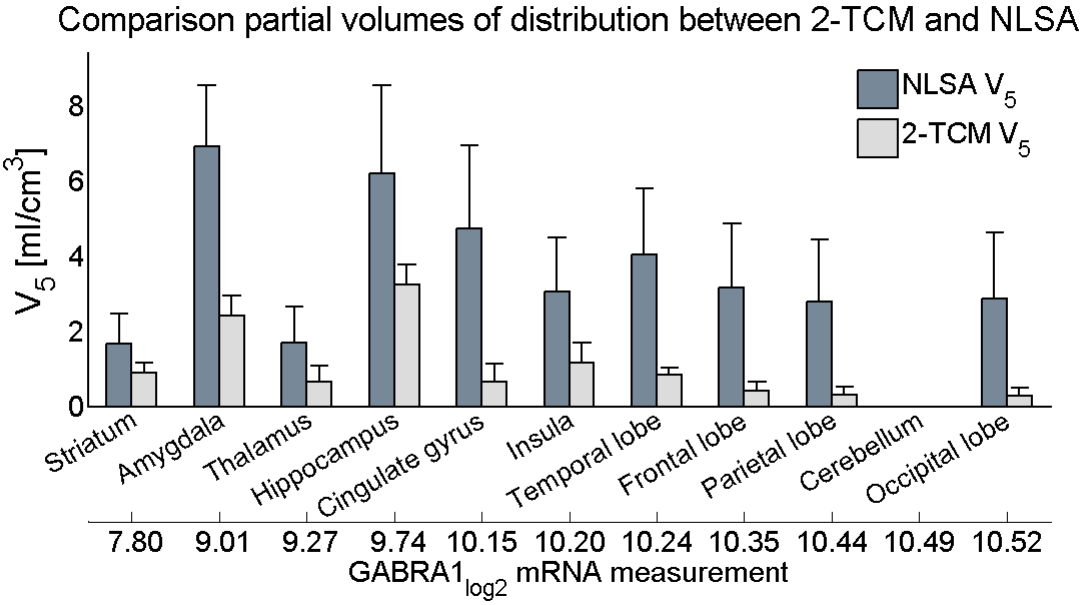

(a) Order of the ROIs due to GABRA1 expression.

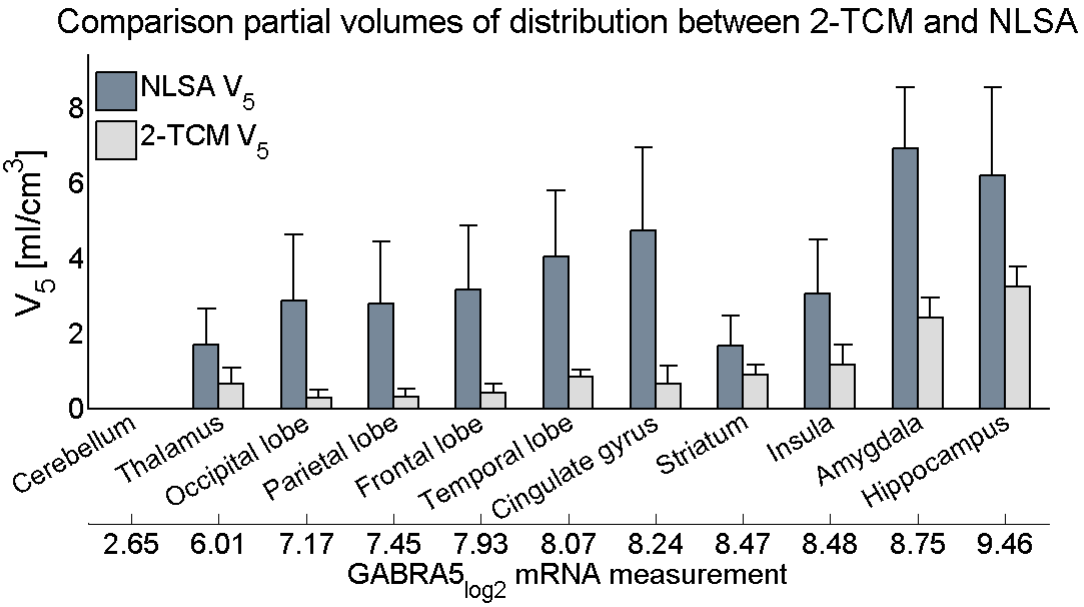

(b) Order of the ROIs due to GABRA5 expression.

Figure 4.11: Comparison of V_5 sorted according to the expressions of the GABA genes.

4.4 Discussion and conclusion

The model underlying [^{11}C]Ro15-4513 is the full receptor model (3-TCM). The free tracer, non-specific receptors and low-specific α receptors have similar kinetics and thus they are difficult to separate. Consequently, the model collapse to a 2-TCM.

2-TCM and 3-TCM identify the same specific binding kinetics (related to GABA-A receptors with α_5 subunit since the tracer has the highest affinity for them). Instead, the contributions of the low-specific α subtypes can not be directly extracted from the tissue activity curve.

In the placebo-zolpidem data set little or no variations are found for V_t while a notable decrease in V_1 and a remarkable increase in V_5 are reported. These results are in agreement with the effects of zolpidem administration: GABA-A receptors containing α_1 subtype are occupied by the drugs and this results in a higher apparent affinity of the tracer resulting in an increment of V_5.

A high correlation is found between V_5 of 2-TCM and GABRA5 (ρ^2=0.84), i.e. the gene related to α_5 subunit, while a smaller value is obtained with NLSA (ρ^2=0.37).

Thus, 2-TCM can properly quantify the α_5 receptor density from [^{11}C]Ro15-4513 PET images, while spectral methods provide only an indirect measure.

As regards V_1, it does not describe a specific α subtype since several factors contribute to it. However, a considerable Spearman's ρ^2 are reported between 2-TCM V_1 and GABRA3 (ρ^2=0.73).

Therefore, 2TCM is the suggested model for the quantification of the α_5 receptor density measured with [^{11}C]Ro15-4513 data at ROI level.

Chapter 5

Quantification results: simplified reference tissue model

The BP_{ND} calculated with the SRTM is compared to those derived with 2-TCM ("direct", Equation 2.13; "indirect", Equation 2.26) and to the 2-TCM V_5.

The correlation plots of three subjects representing the best, the average and the worst case (from placebo, zolpidem and test dataset respectively) are reported for each comparison. The choice of the subjects is due to previous results (such as goodness-of-fit and number of non-reliable ROIs) and the correlation values obtained in this chapter.

Non-reliable "direct" BP_{ND}s, i.e. those with CV higher than 50%, are removed from the analysis: 41% in the healthy data set and 26% in the placebo-zolpidem data set. In the healthy data set, the majority of them belongs to the first and the fourth subject (76%).

As regards the "indirect" BP_{ND} and the V_5, same outliers are removed as in section 4.2.2 (healthy data set) and 4.2.3 (placebo-zolpidem data set) that is the ROIs with CV of V_t higher than 50%.

"Direct" binding potential Limited correlations are obtained in most subjects of healthy and placebo-zolpidem data set (Figure 5.1, Table 5.1 and 5.2).

A high correlation in the fifth subject after zolpidem administration is reported (R^2=0.92), however 13 ROIs (77%) are removed.

"Indirect" binding potential High correlations (R^2>0.98) are obtained for all subjects of the heathy and the placebo-zolpidem data set when comparing SRTM and the "indirect" BP_{ND} (Figure 5.2).

Volume of distribution Lastly, the correlations between the V_5 calculated with 2-TCM and the SRTM BP_{ND} are reported (Figure 5.3).

Overall, high R^2s are found in both dataset. Interestingly, the lowest values are obtained in the first and in the fourth subject of the healthy data set in agreement with the problems in their fitting. Moreover, the correlation of the

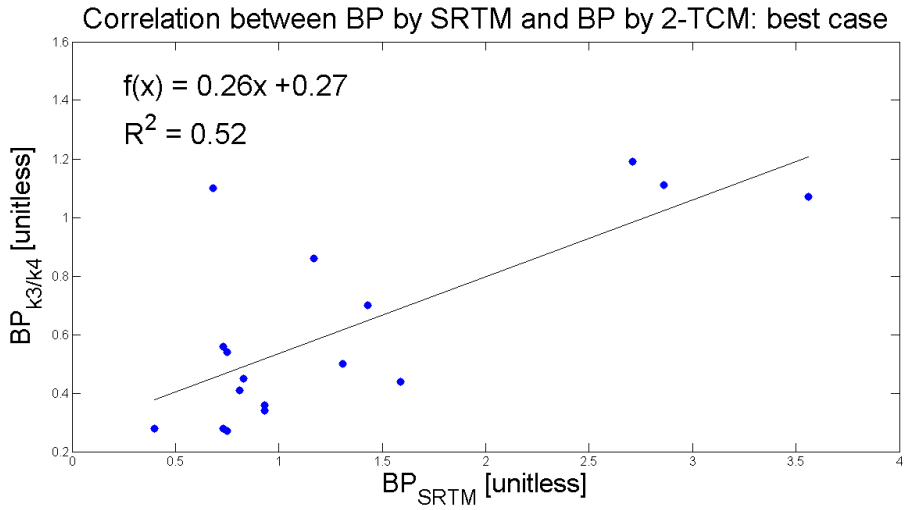

(a) Correlation of the second subject of the placebo data set.

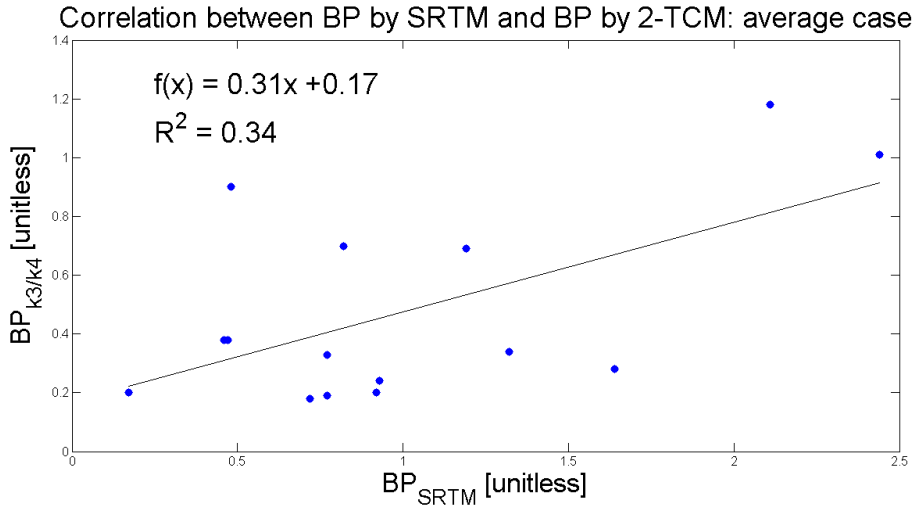

(b) Correlation of the first subject of the zolpidem data set.

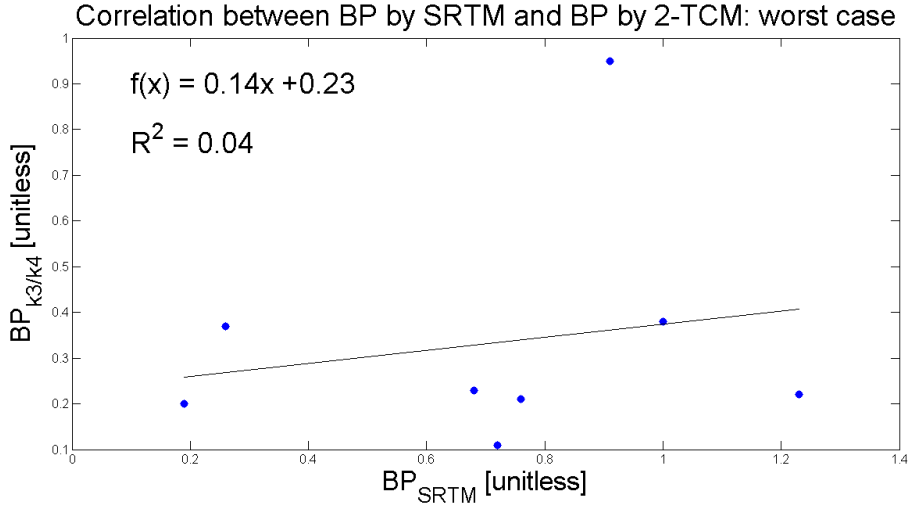

(c) Correlation of the first subject of the healthy data set.

Figure 5.1: Correlations between BPs obtained with 2-TCM and SRTM in three subjects.

	k3/k4 [*unitless*]	DVR-1 [*unitless*]	V5 [ml/cm^3]
Test H1	0.03	0.99	0.50
Retest H1	0.35	1.00	0.49
Test H2	0.33	1.00	0.71
Retest H2	0.39	0.99	0.80
Test H3	0.45	1.00	0.90
Retest H3	0.16	1.00	0.59
Test H4	0.01	0.99	0.57
Retest H4	0.00	0.98	0.25

Table 5.1: Pearson's R^2 between the BP obtained with SRTM and the three different parameters of interest in the healthy data set.

	k3/k4 [*unitless*]	DVR-1 [*unitless*]	V5 [ml/cm^3]
Placebo 1	0.10	1.00	0.63
Zolpidem 1	0.34	1.00	0.74
Placebo 2	0.53	1.00	0.93
Zolpidem 2	0.53	0.99	0.83
Placebo 3	0.07	1.00	0.62
Zolpidem 3	0.34	1.00	0.89
Placebo 4	0.05	1.00	0.71
Zolpidem 4	0.00	1.00	0.67
Placebo 5	0.10	1.00	0.76
Zolpidem 5	0.92	1.00	0.69

Table 5.2: Pearson's R^2 between the BP obtained with SRTM and the three different parameters of interest in the placebo-zolpidem data set.

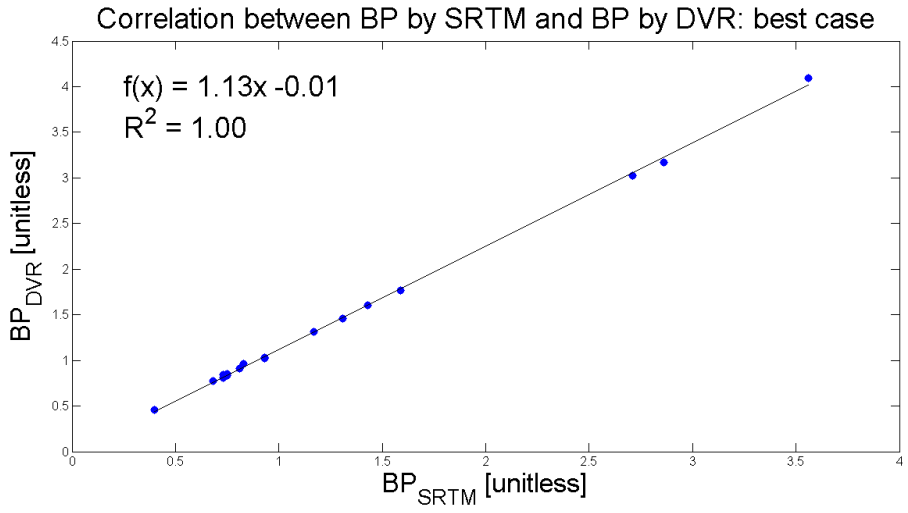

(a) Correlation of the second subject of the placebo data set.

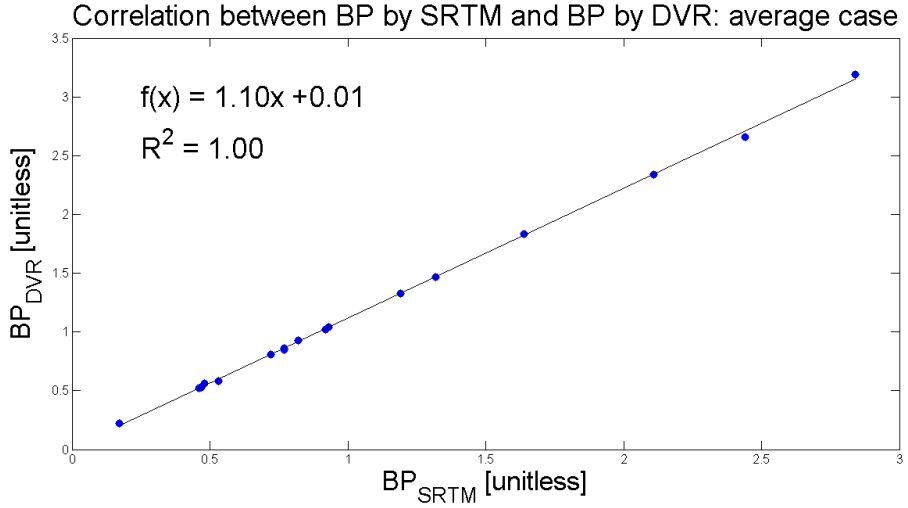

(b) Correlation of the first subject of the zolpidem data set.

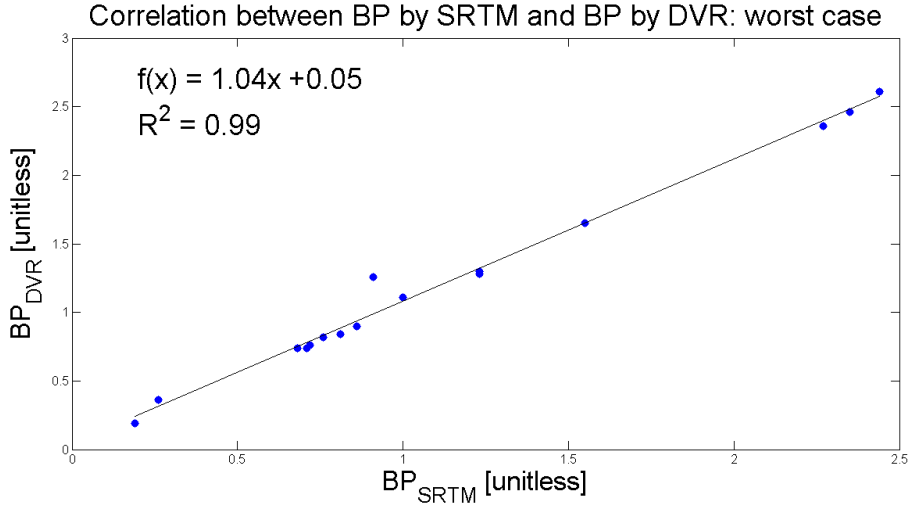

(c) Correlation of the first subject of the healthy data set.

Figure 5.2: Correlations between BPs obtained by means of DVR and SRTM in three subjects.

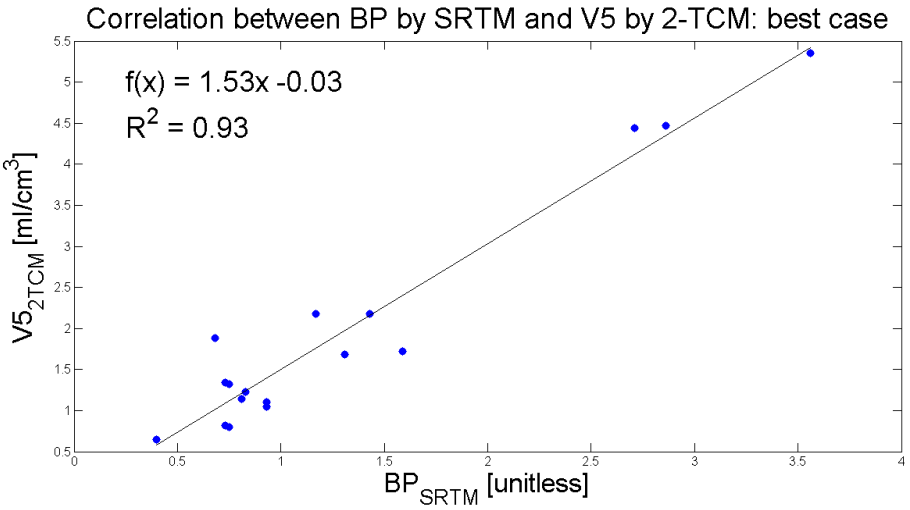

(a) Correlation of the second subject of the placebo data set.

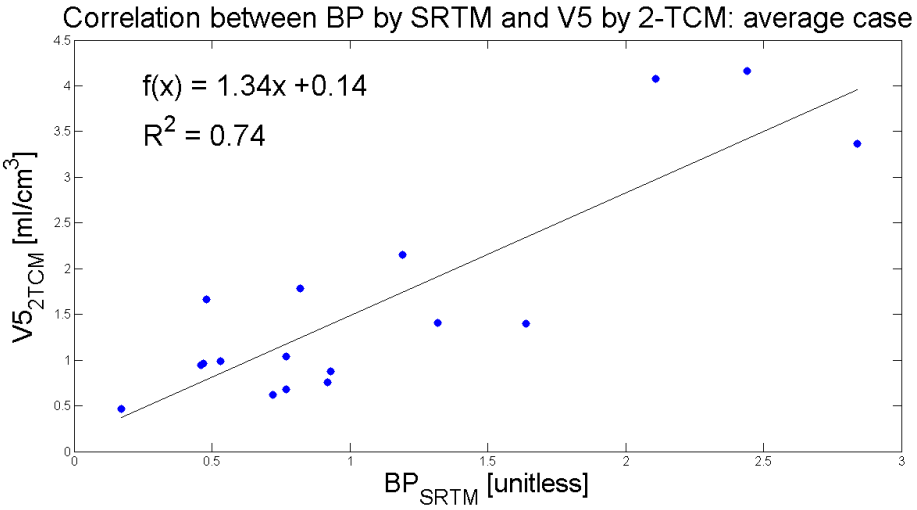

(b) Correlation of the first subject of the zolpidem data set.

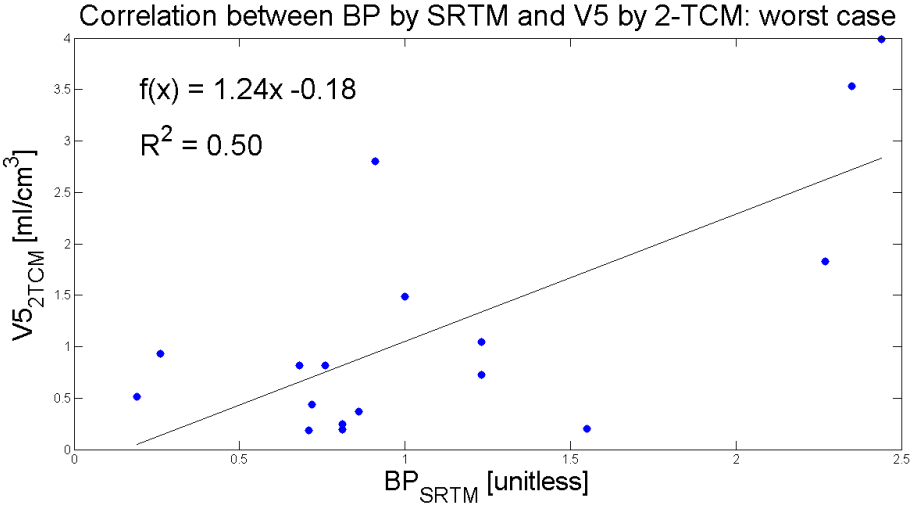

(c) Correlation of the first subject of the healthy data set.

Figure 5.3: Correlations between V5 obtained with 2-TCM an BP calculated by means of SRTM in three subjects.

retest of the fourth subject is very poor because only few regions are reliable (29%).

5.1 Discussion and conclusion

The results can be interpreted on the basis of the SRTM assumptions [22]:

1. the reference region does not contain specific receptors,
2. the level of non-specific binding is the same in the ROI and in the reference tissue,
3. the tracer kinetics can be fitted satisfactorily to a single tissue compartment model with plasma input, without significant improvement when a two-tissue compartment model is used.

While the first assumption is correct because the Cerebellum lacks of α_5 receptors, the second one and the third one are not valid for the tracer under study: the non-displaceable compartment contains the low-specific α receptors thus its contribution is different in each region. Furthermore, the 2-TCM significantly improves the fit and the weighted residuals compared to 1-TCM in several regions.

These considerations explain the low correlations found with the "direct" BP_{ND}.

On the contrary, the BP_{ND} derived by DVR is calculated indirectly from the volumes of distribution of the ROI and the reference region. The Equation 2.26 can be rewritten as:

$$BP_{ND} = DVR - 1 \tag{5.1}$$

$$= \frac{V_t - V_{t_{ref}}}{V_{t_{ref}}} \tag{5.2}$$

$$= \frac{\frac{K_1}{k_2}\left[1 + \frac{k_3}{k_4}\right] - \frac{K_1'}{k_2'}}{\frac{K_1'}{k_2'}} \tag{5.3}$$

where K_1, k_2, k_3 and k_4 are the kinetic parameters of the ROI while K_1' and k_2' are related to the reference region.

Therefore, "indirect" BP_{ND} is equal at $\frac{k_3}{k_4}$ only if $\frac{K_1}{k_2}$ is equal at $\frac{K_1'}{k_2'}$.

As seen above, the V_1, i.e. $\frac{K_1}{k_2}$, is different for each ROI therefore the "indirect" BP_{ND} is not equal at $\frac{k_3}{k_4}$ but it is highly correlated to the BP obtained with the SRTM. The little difference between them might be due to the third assumption of the SRTM.

Lastly, good correlations are found between the V_5 of the 2-TCM and the BP_{ND} by SRTM.

Therefore, the BP calculated with SRTM might be used to obtain a value highly correlated to the α_5 content (described by V_5 and "indirect" BP_{ND}) in particular for the subjects in which the 2-TCM gives reliable and physiological results.

However, further studies should be done to assess this possibility.

Chapter 6

Voxel-wise results

Parametric maps of a representative subject are obtained with 2-TCM and NLSA in order to evaluate the different spatial distribution of the V_t and the V_5 in sections of particular interest (Figure 6.1 and 6.2).

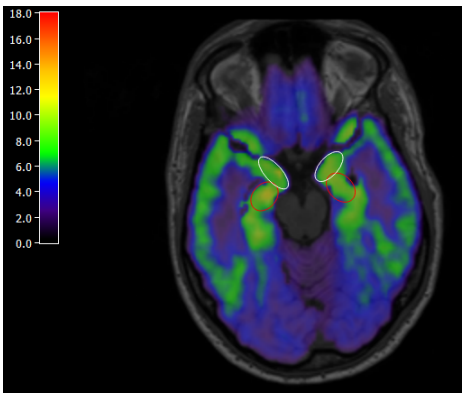

(a) V_t obtained with NLSA

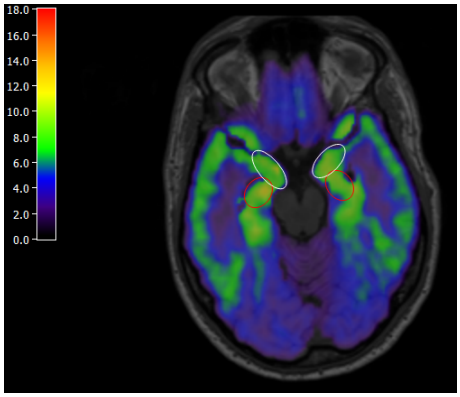

(c) V_t obtained with 2TCM

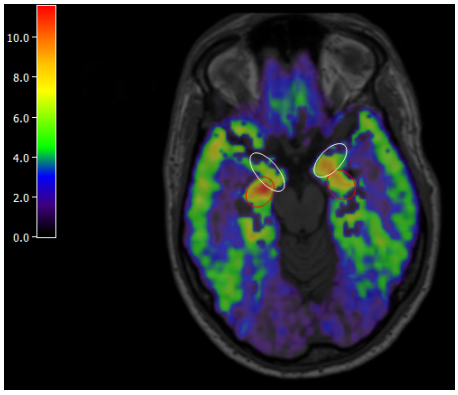

(b) V_5 obtained with NLSA

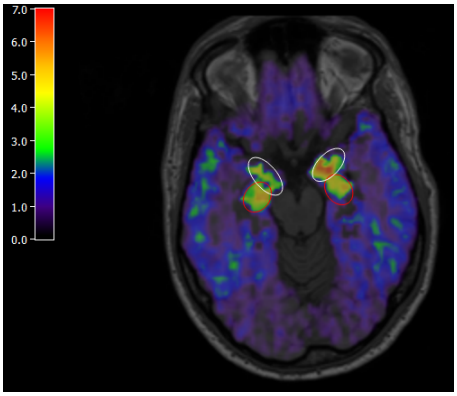

(d) V_5 obtained with 2TCM

Figure 6.1: Axial section of V_t and V_5 obtained with NLSA and 2-TCM of a representative subject. Red ellipse is Hippocampus while white ellipse is Amygdala.

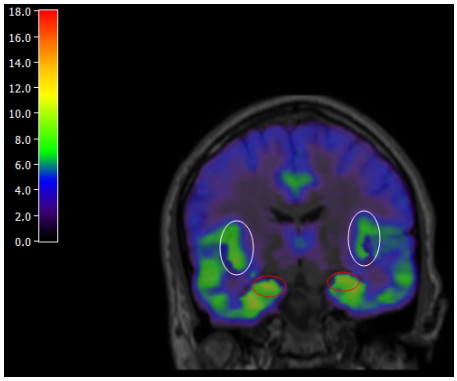

(a) V_t obtained with NLSA

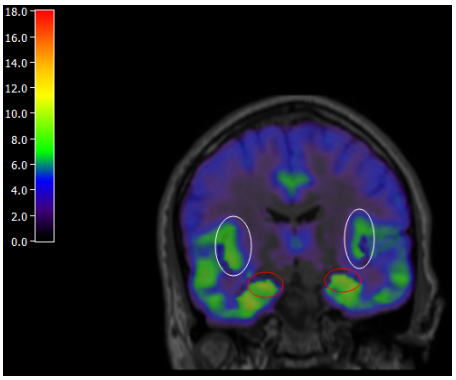

(c) V_t obtained with 2TCM

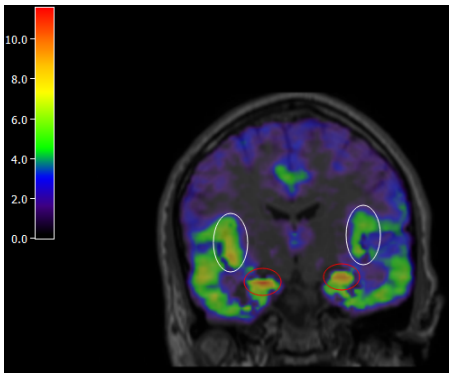

(b) V_5 obtained with NLSA

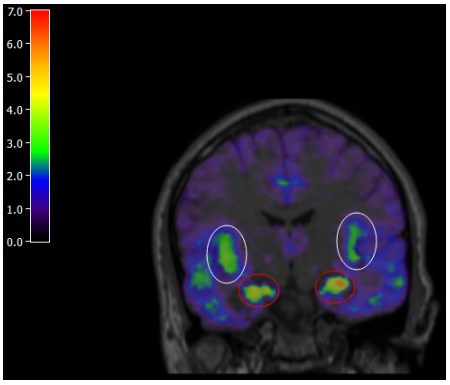

(d) V_5 obtained with 2TCM

Figure 6.2: Coronal section of V_t and V_5 obtained with NLSA and 2-TCM of a representative subject. Red ellipse is Hippocampus while white ellipse is Insula.

Voxel-wise parametric maps confirm ROI-level results: the V_ts obtained with NLSA and 2TCM are almost equal while notable differences are found in V_5.

The spatial distribution of 2TCM V_5 is in agreement with that of GABA-A receptors containing α_5 subtypes. In fact, high values are found in Hippocampus, Amygdala and Insula (Figure 6.1d and 6.2d).

Instead, NLSA V_5 has a wider distribution compared to 2-TCM because it is a "mixture" of model compartments and thus it does not directly describe the specific binding.

Therefore, 2-TCM can be applied at voxel level to obtain parametric maps of [^{11}C]Ro15-4513 in order to study the distribution of α_5 receptors.

Chapter 7

Conclusion

GABA-A receptors containing α_5 subunits are involved in several important aspects such as learning and memory. Their expression is related to diseases that affect the brain as, for example, Alzheimer.

[^{11}C]Ro15-4513 has a high affinity for α_5 receptors however other α subtypes contribute to the tissue activity curve and thus mathematical models are needed to extract the information regarding the α_5 subtype.

In this study, two different techniques were applied to isolate α_5 contribution: data-driven and model-driven methods.

As regards data-driven methods, NLSA outperformed LSA in several aspects: number of components estimated, fit, weighted residuals and repeatability. Therefore, it is preferable to LSA for the quantification of the total volume of distribution of [^{11}C]Ro15-4513 data at ROI level.

Afterwards, model-driven methods were used to study the specific binding of α_5 receptors: with 3-TCM and 2-TCM it is possible to derive the distribution of GABA-A receptors containing α_5 subunit. Instead, the partial volumes of distribution obtained with spectral methods are a "mixture" of the model compartments and thus they can not be used to achieve the distribution of a specific α subtype.

In fact, the mRNA level of the gene related to α_5 receptors was highly correlated with V_5 of 2-TCM while poor correlated with NLSA V_5.

Subsequently, the SRTM was used to assess its applicability: good correlations were found between SRTM BP_{ND} and 2-TCM V_5. Therefore, it might be used to derive the α_5 content of the PET data.

Preliminary voxel-wise analysis confirmed the ROI-level results: the spatial distribution of 2-TCM V_5 was in agreement with that of α_5 receptors. Thus, parametric maps might be used to evaluate their expression.

Appendix A

Region list

A.1 PET atlas region list

1. Hippocampus right
2. Hippocampus left
3. Amygdala right
4. Amygdala left
5. Anterior temporal lobe, medial part right
6. Anterior temporal lobe, media part left
7. Anterior temporal lobe, lateral part right
8. Anterior temporal lobe, lateral part left
9. Parahippocampal and ambient gyri right
10. Parahippocampal and ambient gyri left
11. Superior temporal gyrus right
12. Superior temporal gyrus left
13. Middle and inferior temporal gyri right
14. Middle and inferior temporal gyri left
15. Fusiform gyrus right
16. Fusiform gyrus left
17. Cerebellum right
18. Cerebellum left
19. Brainstem
20. Insula left
21. Insula right
22. Lateral remainder of occipital lobe left
23. Lateral remainder of occipital lobe right
24. Gyrus cinguli, anterior part left
25. Gyrus cinguli, anterior part right
26. Gyrus cinguli, posterior part left
27. Gyrus cinguli, posterior part right
28. Middle frontal gyrus left
29. Middle frontal gyrus right
30. Posterior temporal lobe right
31. Posterior temporal lobe left

32. Inferolateral remainder of parietal lobe left
33. Inferolateral remainder of parietal lobe right
34. Caudate nucleus left
35. Caudate nucleus right
36. Nucleus accumbens left
37. Nucleus accumbens right
38. Putamen left
39. Putamen right
40. Thalammus left
41. Thalamus right
42. Pallidum left
43. Pallidum right
44. Corpus callosum
45. Lateral ventricle (excluding temporal horn) right
46. Lateral ventricle (excluding temporal horn) left
47. Lateral ventricle, temporal horn right
48. Lateral ventricle, temporal horn left
49. Third ventricle
50. Precentral gyrus left
51. Precentral gyrus right
52. Gyrus rectus left
53. Gyrus rectus right
54. Orbitofrontal gyri left
55. Orbitofrontal gyri right
56. Inferior frontal gyrus left
57. Inferior frontal gyrus right
58. Superior frontal gyrus left
59. Superior frontal gyrus right
60. Postcentral gyrus left
61. Postcentral gyrus right
62. Superior parietal gyrus left
63. Superior parietal gyrus right
64. Lingual gyrus left
65. Lingual gyrus right
66. Cuneus left
67. Cuneus right

A.2 Region of interest list

Name	Atlas region list number
Whole Brain	all regions
Hippocampus	1-2
Amygdala	3-4
Cerebellum	17-18
Insula	20-21
Caudate	34-35
Putamen	38-39
Striatum	34-39
Accumbens	36-37
Thalamus	40-41
Pallidum	42-43
Cingulate	24-27
Parietal lobe	32-33, 52-53, 60-63
Occipital lobe	22-23, 64-67
Temporal lobe	5-16, 30-31
Frontal lobe	28-29, 50-51, 54-59
Subcortical	1-4, 34-35, 38-39, 42-43
Cortical	5-16, 22-23, 28-33, 50-67

A.3 Allen atlas coarse regions

1. Frontal lobe
2. Insula
3. Cingulate gyrus
4. Hippocampal formation
5. Parahippocampal gyrus
6. Occipital lobe
7. Parietal lobe
8. Temporal lobe
9. Amygdala
10. Basal forebrain
11. Globus pallidus
12. Striatum
13. Claustrum
14. Epithalamus
15. Hypothalamus
16. Subthalamus
17. Dorsal thalamus
18. Ventral thalamus
19. Mesencephalon
20. Cerebellar cortex
21. Cerebellar nuclei
22. Basal part of pons
23. Pontine tegmentum
24. Myelencephalon
25. White matter
26. Sulci and spaces

A.4 PET region of interest and Allen region relation

Region of interest	**Allen region**
Hippocampus	Hippocampal formation and Parahippocampal gyrus
Amygdala	Amygdala
Cerebellum	Cerebellar cortex and Cerebellar nuclei
Insula	Insula
Caudate	No one
Putamen	No one
Striatum	Striatum
Accumbens	No one
Thalamus	Epithalamus, Hypothalamus, Subthalamus, Dorsal thalamus and Ventral thalamus
Pallidum	Globus pallidus
Cingulate	Cingulate gyrus
Parietal lobe	Parietal lobe
Occipital lobe	Occipital lobe
Temporal lobe	Temporal lobe
Frontal lobe	Frontal lobe
Subcortical	No one
Cortical	No one

Appendix B

Genomic integration histograms

B.1 Total volume of distribution

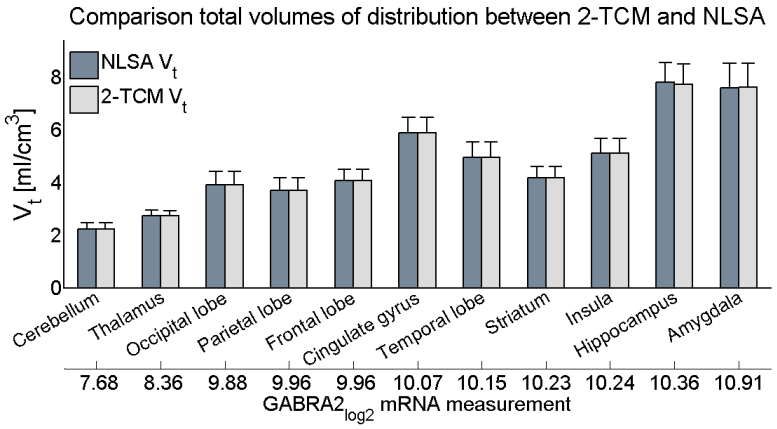

(a) Order of the ROIs due to GABRA2 expression.

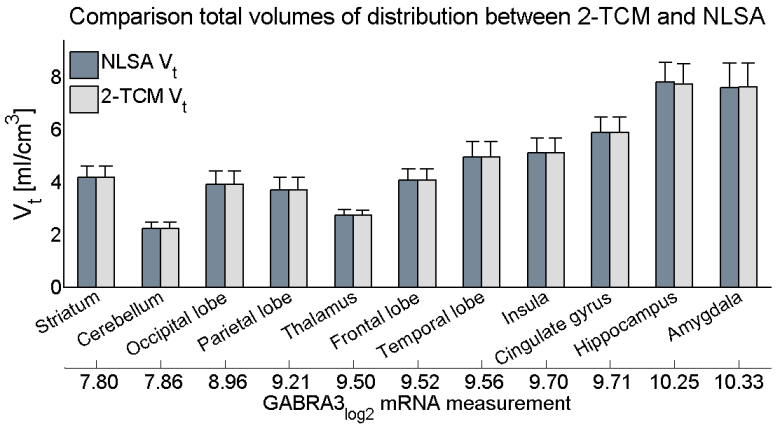

(b) Order of the ROIs due to GABRA3 expression.

Figure B.1: Comparison of V_t sorted according to the expressions of the GABA genes.

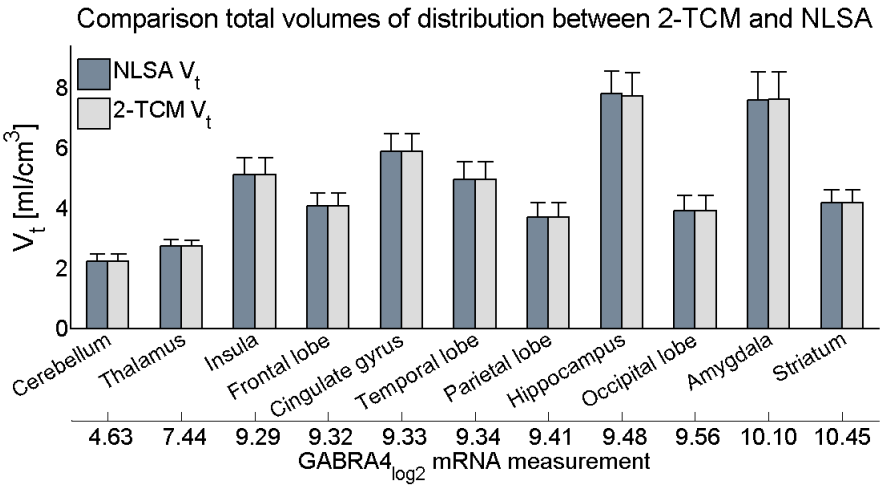

(c) Order of the ROIs due to GABRA4 expression.

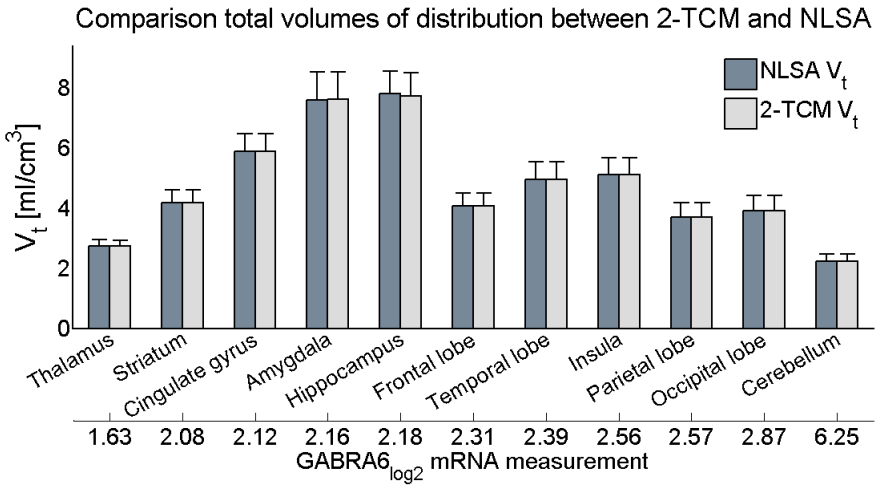

(d) Order of the ROIs due to GABRA6 expression.

Figure B.1: Comparison of V_t sorted according to the expressions of the GABA genes.

B.2 First partial volume of distribution

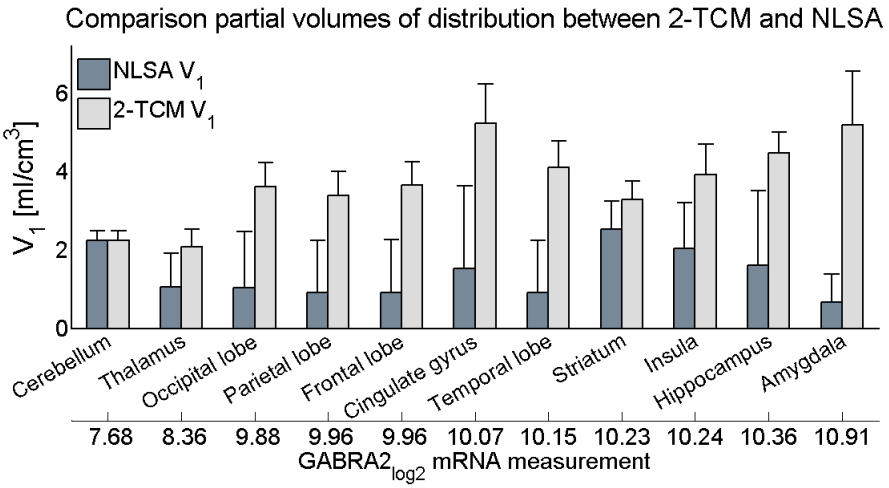

(a) Order of the ROIs due to GABRA2 expression.

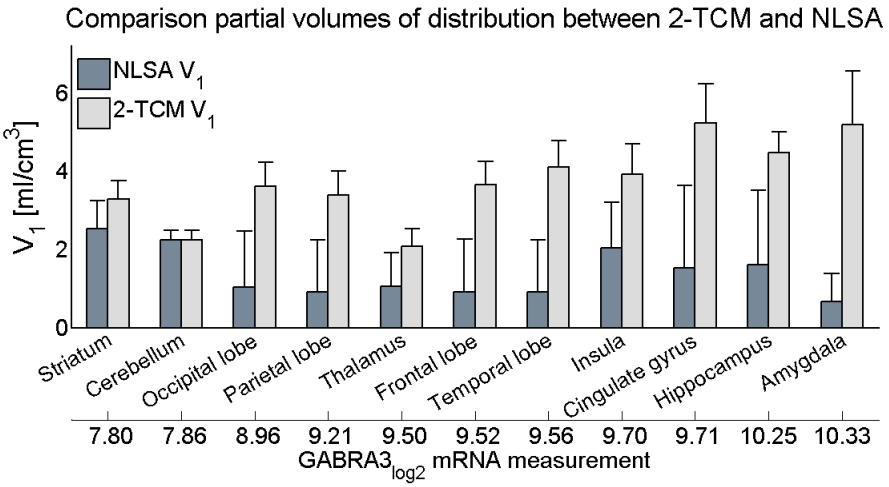

(b) Order of the ROIs due to GABRA3 expression.

Figure B.2: Comparison of V_1 sorted according to the expressions of the GABA genes.

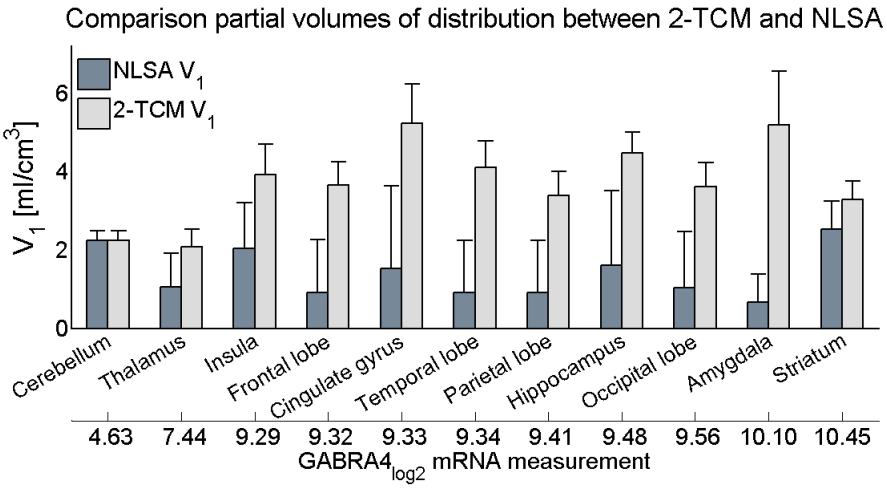

(c) Order of the ROIs due to GABRA4 expression.

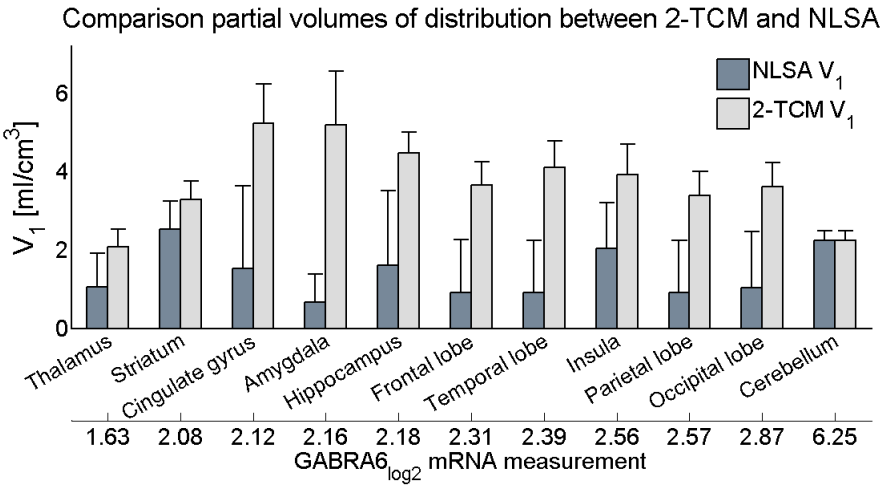

(d) Order of the ROIs due to GABRA6 expression.

Figure B.2: Comparison of V_1 sorted according to the expressions of the GABA genes.

B.3 Second partial volume of distribution

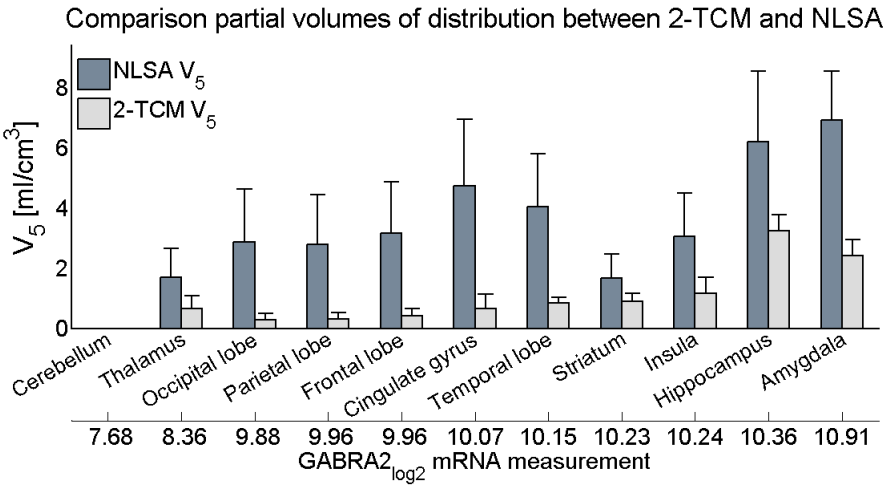

(a) Order of the ROIs due to GABRA2 expression.

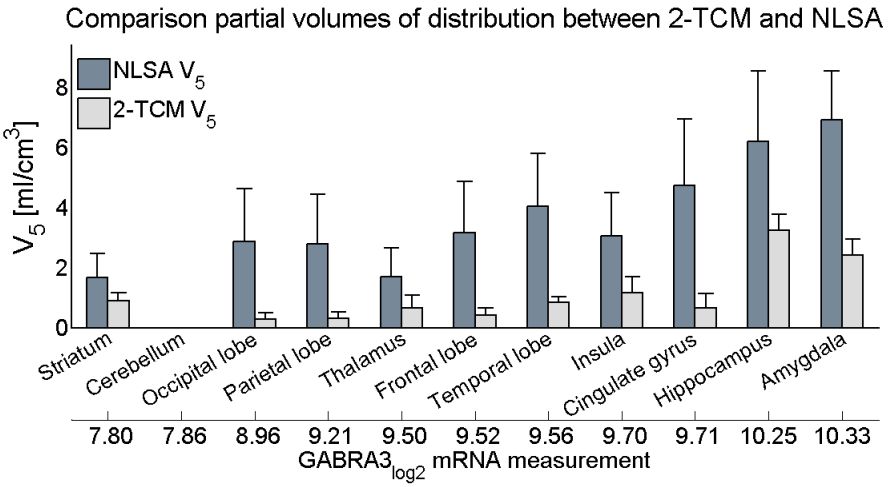

(b) Order of the ROIs due to GABRA3 expression.

Figure B.3: Comparison of V_5 sorted according to the expressions of the GABA genes.

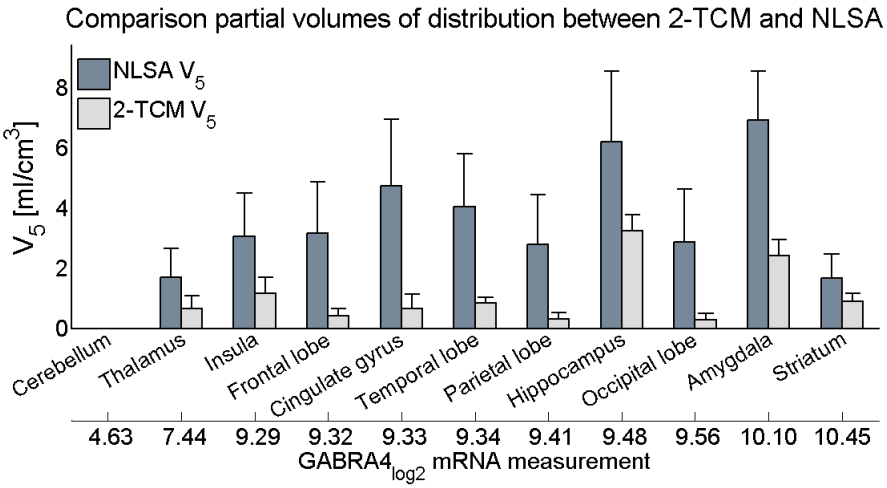

(c) Order of the ROIs due to GABRA4 expression.

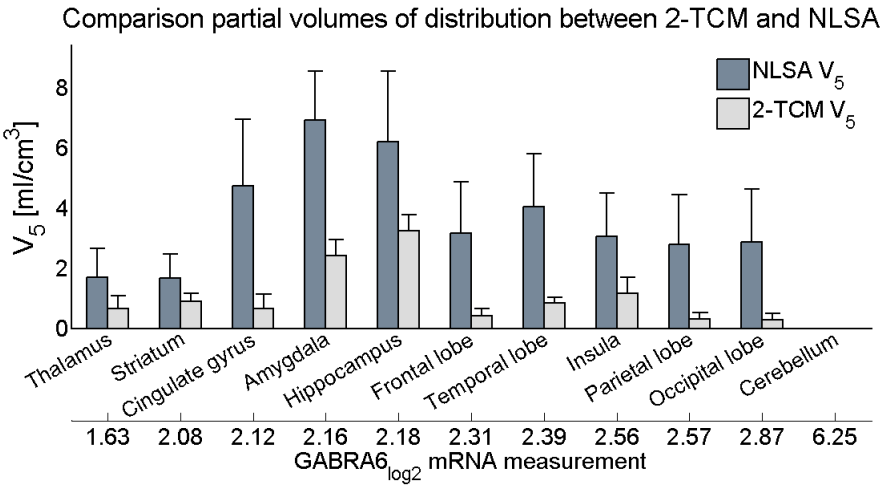

(d) Order of the ROIs due to GABRA6 expression.

Figure B.3: Comparison of V_5 sorted according to the expressions of the GABA genes.

Bibliography

[1] R. M. McKernan and P. J. Whiting. Which gaba-a receptor subtypes really occur in the brain? *Trends in neurosciences* 19(4):139–143, 1996.

[2] C. D'Hulst, J. R. Atack, and R. F. Kooy. The complexity of the gaba-a receptor shapes unique pharmacological profiles. *Drug discovery today* 14(17):866–875, 2009.

[3] H. Möhler, J. Fritschy, and U. Rudolph. A new benzodiazepine pharmacology. *Journal of Pharmacology and Experimental Therapeutics* 300(1):2–8, 2002.

[4] K. A. Wafford. GABA-A receptor subtypes: any clues to the mechanism of benzodiazepine dependence? *Current opinion in pharmacology* 5(1):47–52, 2005.

[5] P. J. Whiting. Gaba-a receptor subtypes in the brain: a paradigm for cns drug discovery? *Drug discovery today* 8(10):445–450, 2003.

[6] S. Pirker, C. Schwarzer, A. Wieselthaler, W. Sieghart, and G. Sperk. Gaba-a receptors: immunocytochemical distribution of 13 subunits in the adult rat brain. *Neuroscience* 101(4):815–850, 2000.

[7] W. Sieghart and G. Sperk. Subunit composition, distribution and function of gaba-a receptor subtypes. *Current topics in medicinal chemistry* 2(8):795–816, 2002.

[8] F. H. Fahey. Positron emission tomography instrumentation. *Radiologic Clinics of North America* 39(5):919–929, 2001.

[9] D. L. Bailey, D. W. Townsend, P. E. Valk, and M. N. Maisey. *Positron emission tomography*. Springer, 2005.

[10] P. R. Stokes, J. F. Myers, N. J. Kalk, B. J. Watson, D. Erritzoe, S. J. Wilson, V. J. Cunningham, D. R. Barros, A. Hammers, F. E. Turkheimer, et al. Acute increases in synaptic GABA detectable in the living human brain: a [^{11}C]Ro15-4513 PET study. *NeuroImage*, 2014.

[11] A. Lingford-Hughes, A. G. Reid, J. Myers, A. Feeney, A. Hammers, L. G. Taylor, L. Rosso, F. Turkheimer, D. J. Brooks, P. Grasby, et al. A [^{11}C]Ro15 4513 PET study suggests that alcohol dependence in man is

associated with reduced α_5 benzodiazepine receptors in limbic regions. *Journal of Psychopharmacology* 26(2):273–281, 2012.

[12] J. F. Myers, L. Rosso, B. J. Watson, S. J. Wilson, N. J. Kalk, N. Clementi, D. J. Brooks, D. J. Nutt, F. E. Turkheimer, and A. R. Lingford-Hughes. Characterisation of the contribution of the GABA-benzodiazepine α_1 receptor subtype to [^{11}C]Ro15-4513 PET images. *Journal of Cerebral Blood Flow & Metabolism* 32(4):731–744, 2012.

[13] H. Wang, J. W. Suh, S. R. Das, J. B. Pluta, C. Craige, and P. A. Yushkevich. Multi-atlas segmentation with joint label fusion. *Pattern Analysis and Machine Intelligence, IEEE Transactions on* 35(3):611–623, 2013.

[14] M.-C. Asselin, A. J. Montgomery, P. M. Grasby, and S. P. Hume. Quantification of pet studies with the very high-affinity dopamine d2/d3 receptor ligand [11c] flb 457: re-evaluation of the validity of using a cerebellar reference region. *Journal of Cerebral Blood Flow & Metabolism* 27(2):378–392, 2006.

[15] M. Veronese, R. N. Gunn, S. Zamuner, and A. Bertoldo. A non-linear mixed effect modelling approach for metabolite correction of the arterial input function in PET studies. *NeuroImage* 66:611–622, 2013.

[16] M. Tonietto. Methods and models for the characterization of arterial input function in dynamic PET studies. Master's thesis, University of Padua, 2012. available at http://tesi.cab.unipd.it.

[17] V. J. Cunningham and T. Jones. Spectral analysis of dynamic PET studies. *Journal of Cerebral Blood Flow & Metabolism* 13(1):15–23, 1993.

[18] F. Turkheimer, L. Sokoloff, A. Bertoldo, G. Lucignani, M. Reivich, J. L. Jaggi, and K. Schmidt. Estimation of component and parameter distributions in spectral analysis. *Journal of Cerebral Blood Flow & Metabolism* 18(11):1211–1222, 1998.

[19] K. Schmidt. Which linear compartmental systems can be analyzed by spectral analysis of PET output data summed over all compartments? *Journal of Cerebral Blood Flow & Metabolism* 19(5):560–569, 1999.

[20] A. Bertoldo, P. Vicini, G. Sambuceti, A. A. Lammertsma, O. Parodi, and C. Cobelli. Evaluation of compartmental and spectral analysis models of [^{18}f] fdg kinetics for heart and brain studies with pet. *Biomedical Engineering, IEEE Transactions on* 45(12):1429–1448, 1998.

[21] M. A. Mintun, M. E. Raichle, M. R. Kilbourn, G. F. Wooten, and M. J. Welch. A quantitative model for the in vivo assessment of drug binding sites with positron emission tomography. *Annals of neurology* 15(3):217–227, 1984.

[22] A. A. Lammertsma and S. P. Hume. Simplified reference tissue model for PET receptor studies. *Neuroimage* 4(3):153–158, 1996.

[23] M. R. Dittrich S., Van den Hoff J. PET pharmacokinetic course manual 2010. Loch Lomond, Scotland.

[24] B. M. Mazoyer, R. H. Huesman, T. F. Budinger, and B. L. Knittel. Dynamic PET data analysis. *Journal of computer assisted tomography* 10(4):645–653, 1986.

[25] A. Bertoldo, P. Vicini, G. Sambuceti, A. A. Lammertsma, O. Parodi, and C. Cobelli. Evaluation of compartmental and spectral analysis models of [^{18}f]FDG kinetics for heart and brain studies with PET. *Biomedical Engineering, IEEE Transactions on* 45(12):1429–1448, 1998.

[26] G. Rizzo, F. E. Turkheimer, and A. Bertoldo. Multi-scale hierarchical approach for parametric mapping: Assessment on multi-compartmental models. *NeuroImage* 67:344–353, 2013.

[27] W. Sieghart. Structure and pharmacology of γ-aminobutyric acida receptor subtypes. *Pharmacological Reviews* 47(2):181–234, 1995.

[28] M. J. Hawrylycz, E. S. Lein, A. L. Guillozet-Bongaarts, E. H. Shen, L. Ng, J. A. Miller, L. N. van de Lagemaat, K. A. Smith, A. Ebbert, Z. L. Riley, et al. An anatomically comprehensive atlas of the adult human brain transcriptome. *Nature* 489(7416):391–399, 2012.

[29] G. Rizzo, M. Veronese, R. A. Heckemann, S. Selvaraj, O. D. Howes, A. Hammers, F. E. Turkheimer, and A. Bertoldo. The predictive power of brain mRNA mappings for in vivo protein density: a positron emission tomography correlation study. *Journal of Cerebral Blood Flow & Metabolism* 34(5):827–835, 2014.

[30] M. A. Mendez, J. Horder, J. Myers, S. Coghlan, P. Stokes, D. Erritzoe, O. Howes, A. Lingford-Hughes, D. Murphy, and D. Nutt. The brain GABA-benzodiazepine receptor α5 subtype in autism spectrum disorder: A pilot [^{11}C]Ro15-4513 positron emission tomography study. *Neuropharmacology* 68:195–201, 2013.

[31] D. Barros, R. Heckemann, L. Rosso, C. McGinnity, S. Keihaninejad, I. Gousias, D. Brooks, J. Duncan, M. Koepp, F. Turkheimer, and A. Hammers. Investigating the reproducibility of the novel α_5 GABA-A receptor PET ligand [^{11}C]Ro15-4513. *NeuroImage* 52(S1):S112–S112, 2010.

[32] A. Lingford-Hughes, S. P. Hume, A. Feeney, E. Hirani, S. Osman, V. J. Cunningham, V. W. Pike, D. J. Brooks, and D. J. Nutt. Imaging the GABA-benzodiazepine receptor subtype containing the α_5-subunit in vivo with [^{11}C]Ro15 4513 positron emission tomography. *Journal of Cerebral Blood Flow & Metabolism* 22(7):878–889, 2002.